Strontium isotope stratigraphy and paleomagnetic age constraints on the evolution history of coral reef islands, northern South China Sea

Tianlai Fan[1,2,3], Kefu Yu[1,2,3,†], Jianxin Zhao[4], Wei Jiang[1,2,3], Shendong Xu[1,2,3], Yu Zhang[1,2,3], Rui Wang[1,2,3], Yinghui Wang[1,2,3], Yuexing Feng[4], Lizeng Bian[5], Handong Qian[5], and Weihua Liao[6]

[1]Guangxi Laboratory on the Study of Coral Reefs in the South China Sea, Guangxi University, Nanning, Guangxi 530004, China
[2]Coral Reef Research Center of China, Guangxi University, Nanning, Guangxi 530004, China
[3]School of Marine Sciences, Guangxi University, Nanning, Guangxi 530004, China
[4]School of Earth & Environmental Sciences, The University of Queensland, Brisbane, Queensland 4072, Australia
[5]School of Earth Sciences and Engineering, Nanjing University, Nanjing, Jiangsu 210093, China
[6]Nanjing Institute of Geology and Palaeontology, Chinese Academy of Sciences, Nanjing, Jiangsu 210008, China

ABSTRACT

Understanding the history of the response of coral reefs to past climate changes can provide valuable information for predicting the future response of modern reefs. However, dating such ancient biotic carbonate is still challenging because of its sensitivity to diagenetic alteration processes, scarcity of well-preserved fossils, and low magnetic mineral content. There have been a long debates about the origin and evolutionary history of coral reefs in the northern South China Sea, mainly due to the lack of direct and reliable age constraints. This provides us with a good opportunity to verify the practicability of different dating approaches, especially the strontium (Sr) isotope analysis of bulk carbonate. Here, we retrieved a 972.55-m-long core from the Xisha Islands to provide a credible chronologic constraint on the carbonate platform evolution. The lithostratigraphy, strontium isotope stratigraphy, and magnetostratigraphy were analyzed throughout the whole reef sequence. The lithostratigraphic results show that the 873.55 m reef sequence developed on an ancient volcaniclastic basement and experienced multiple evolutionary phases. The $^{87}Sr/^{86}Sr$ results of all 100 bulk carbonate samples vary from 0.708506 to 0.709168 and show a monotonic increase with decreasing depth, except for a few outliers. Trace-element criteria and stable isotope ($\delta^{18}O$ and $\delta^{13}C$) methods were applied to these bulk carbonate samples, and results imply that the primary or near-primary seawater $^{87}Sr/^{86}Sr$ values were likely preserved, although different degrees of diagenetic alteration occurred. In addition, the paleomagnetic results indicate 10 normal polarity and eight reversed polarity magnetozones. Based on the $^{87}Sr/^{86}Sr$ ratios of the selected 58 samples and paleomagnetic reconstruction of polarity reversals, the bottom of the reef sequence is dated to 19.6 Ma, and the observed polarity chronozones extend from chron C6 (19.722–18.748 Ma) at 866.60 m to present at the top. Based on the new data, we propose a new chronologic framework for the evolutionary history of the reef islands, where: (1) the reefs initiated in the early Miocene (19.6 Ma) and were drowned until 16.26 Ma; (2) during 16.26–10.66 Ma, lagoon to lagoon slope environments prevailed; (3) the lagoon environment progressively transformed into a reef crest environment from 10.66 to 4.36 Ma and 4.36 to 1.59 Ma; and (4) the reef started to be drowned again during 1.59–0 Ma. Our study provides a new and reliable chronologic constraint on the general evolutionary history of the reef islands in the northern South China Sea. Furthermore, the $^{87}Sr/^{86}Sr$ results from bulk carbonate indicate that strontium isotope stratigraphy is a powerful dating tool only when rigid sample selection, sequential leaching procedures, and strict trace-element and isotopic criteria are applied.

INTRODUCTION

Tropical coral reefs are both biological and geological constructions, and so they have long been used by both geologists and biologists to trace past marine ecological and climate change. Indeed, over geological time, coral reefs have suffered dramatic decline as a result of climate change, with multiple expansions and contractions in reef growth associated with environmental drivers as indicated by paleoecological studies and fossil records (Kiessling, 2009; Pandolfi, 2015, and references therein). Particularly, the origin and evolution of coral reefs become priority issues because they can provide a way to understand how coral reefs respond to climate change. Late in the twentieth century and early in the twenty-first century, several drilling programs were performed, and deep coring through atolls was conducted, especially in the middle of the Pacific Ocean (Ludwig et al., 1988; Lincoln and Schlanger, 1991; Ohde et al., 2002). However, little attention has been paid to the origin and evolution of the coral reef islands in the western Pacific, especially in the South China Sea, although the presence of corals in the South China Sea has been known for centuries.

The origin of the coral reef islands within the South China Sea is poorly understood, largely because of a lack of chronologic data. During the past 50 yr, the geological evolution of the South China Sea, and particularly the reef islands, has captured the interest of a large number of scientists because of the widespread variety of reefs (Ludwig et al., 1988). Several deep reef cores have been obtained from the Xisha Islands (Paracel Islands) and Nansha Islands (Spratly Islands), respectively, in order to investigate the ecological environment and evolutionary history of these reef islands (Qin, 1987; Zhang, 1990; Sun et al., 1996). As we now know, the South China Sea is the largest marginal sea in Asia, and it covers an area over 3 million km^2 (Wang and Li, 2009). The coral reefs in the South China Sea play a critical role in both biodiversity refuge and the global carbon cycle through biological processes over 8000 km^2 and high species richness (hosting

571 known species), which is comparable to the Coral Triangle, despite containing less than 17% of the reef area compared to the Coral Triangle (Huang et al., 2015). However, the origin and evolution of ancient coral reefs/atolls in the South China Sea still remain poorly understood, mainly due to the lack of direct and reliable chronological data. Currently, it is uncertain when the atolls or islands of South China Sea started their growth and demise, whether they experienced the same evolutionary history, and how they responded to past climate changes with broad regional impacts (Xu et al., 2002; Ma et al., 2011; Wu et al., 2014, 2016; Shao et al., 2017). Several scientific wells have been drilled in the past 30 yr, including the Xiyong-1, Xiyong-2, Xichen-1, and Xishi-1 wells (Fig. 1; Qin, 1987; Zhang, 1990; Sun et al., 1996; Qiu and Wang, 2001; Xu et al., 2002). These wells provided abundant information on the lithology, biostratigraphy, sedimentology, and seismology of the islands but also were limited to the analysis of shallow boreholes and/or modern carbonate deposition (He et al., 1986). Some researchers have used seismic data to identify unconformities or boundaries and interpret reef sedimentary sequences based on seismic profiles in combination with wells (Ma et al., 2011; Wu et al., 2014, 2016). Recently, a chronological framework for the Xike-1 well on Shi Island

was constructed, mainly based on biostratigraphy and paleomagnetic dating without reliable absolute age constraints (Yi et al., 2016; Shao et al., 2017). Furthermore, Yi et al. (2018) applied cyclostratigraphy and magnetostratigraphy to the XK-1 well and found that Earth's eccentricity and obliquity played dominant roles in the biogenic reef establishment on orbital to tectonic time scales. Despite extensive studies, there is still a lack of samples of the basement rock and directly overlying basal sediment of the reef sequence. This leaves a large margin of error in the estimated ages of the origin and evolutionary processes, rendering various hypotheses regarding initiation mechanisms and evolution untested.

The other important point is that the chronology of the carbonates before the late Pleistocene is problematic and challenging, especially for reef carbonates. Biostratigraphic dating is often hindered by: (1) the absence or poor preservation of age-definitive biostratigraphic markers; and (2) the poor resolution of high-resolution chronostratigraphy data. Diagenetic alteration and subaerial exposures usually preclude the correlation of marine oxygen and carbon isotope stratigraphy for determining ages. Radiometric dating methods, including U-series and ^{14}C dating, are also restricted because of their limited dating range (Braithwaite et al., 2004;

Cabioch et al., 2008; Hua, 2009). Fortunately, strontium isotope stratigraphy has been improved and has become an important and powerful tool for chronostratigraphic and stratigraphic control for determining both the absolute and relative chronology of Neogene marine carbonates (Burke et al., 1982; DePaolo and Ingram, 1985; Palmer and Elderfield, 1985; DePaolo, 1986; Elderfield, 1986; Hess et al., 1986) and has been successfully applied to the Enewetak Atoll (Ludwig et al., 1988), Kita-daito-jima Atoll (Saller and Koepnick, 1990), Bikini Atoll (Lincoln and Schlanger, 1991), Great Barrier Reef (Ohde and Elderfield, 1992; Alexander et al., 2001; Braithwaite et al., 2004), Funafuti Atoll (Ohde et al., 2002), and Hawaiian Islands (Webster et al., 2010; Faichney et al., 2013). In addition, the observation and study of magnetic minerals in carbonates (McNeill et al., 1988) suggested that reef carbonates carry initial stable remanent magnetization. Therefore, magnetostratigraphy has been quickly adopted in dating ancient carbonate platforms (Lu et al., 1996; Sasaki et al., 2006) and reef sequences, including the Mururoa Atoll (Aïssaoui et al., 1990; Aïssaoui and Kirschvink, 1991), Great Barrier Reef (Braithwaite et al., 2004), New Caledonia (Cabioch et al., 2008), and Tahiti (Lund et al., 2010; Ménabréaz et al., 2010), based on the reconstruction of polarity chron successions.
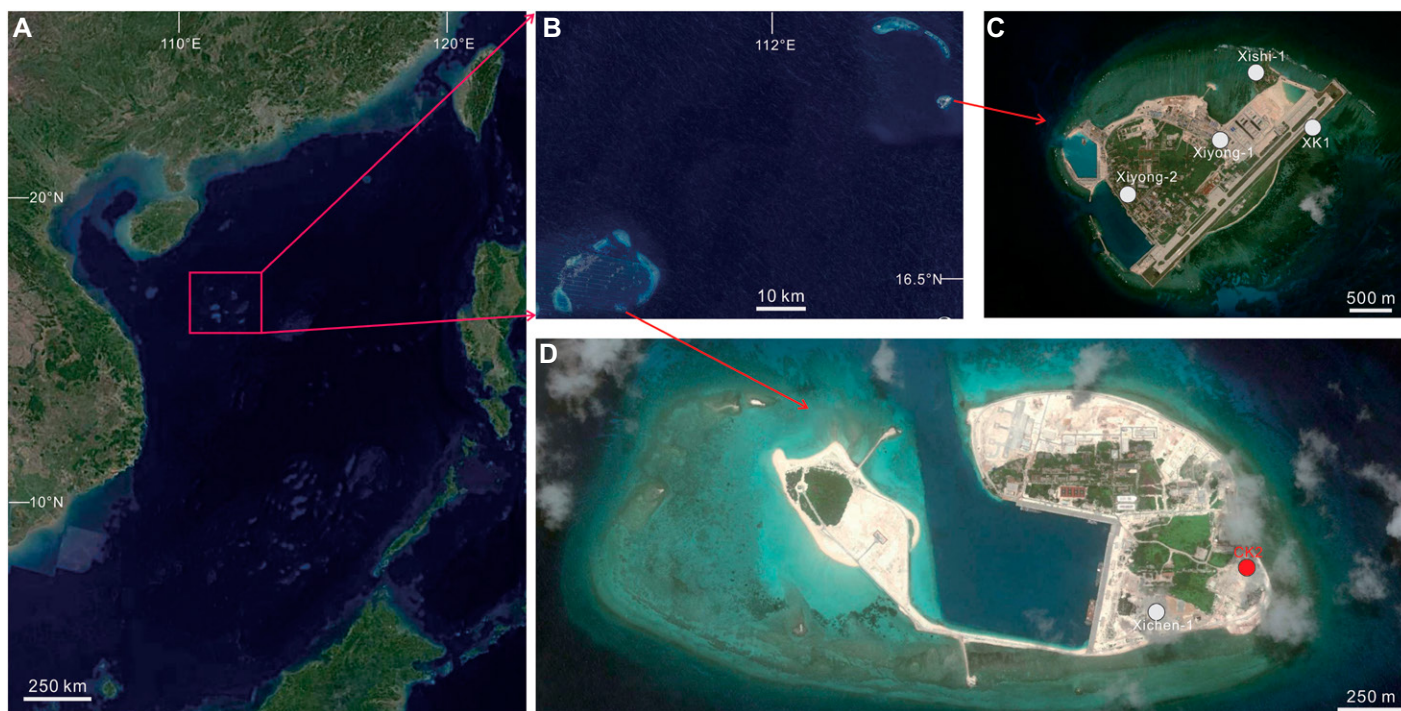
Figure 1. Schematic map of Xisha Island, northern South China Sea, and the distribution of CK2 (filled red circle in D) and previous reef cores (filled white circles in C and D) in the study area. (A) Map of the South China Sea and the location of the Xisha Islands. (B) Map of Yongle Atoll and Xuande Atoll. (C) Yongxing Island and Shidao Island. (D) Map of Chenhang Island and the location of CK2 in our study. All base maps are from Google Earth.

In 2015, a new reef core was retrieved from the Chenke-2 (CK2) well in the Xisha Islands of the northern South China Sea in order to explore the carbonate platform evolution (Fig. 1). Here, we present the lithology, marine $^{87}Sr/^{86}Sr$ stratigraphic age, and magnetostratigraphic age constraints on the carbonate platform evolution of the Xisha Islands. The primary objectives of this study were: (1) to assess the reliability of $^{87}Sr/^{86}Sr$ results of bulk carbonate with different degrees of diagenetic alteration; (2) to contribute to the critical chronostratigraphic control through Sr isotope ages and paleomagnetic results; and (3) to establish a reliable chronostratigraphic framework for the reef evolution. Furthermore, the evolutionary history and geological controls of the reef islands are discussed based on the new chronologic framework.

MATERIALS AND METHODS

Materials and Lithology

The CK2 reef core is considered to be an ideal core because it penetrates the thick reef body and reaches the volcanic basement underlying the reef sequence with a reasonable recovery ratio (928.75 m below surface, 69.6% of the total recovery ratio). The CK2 well consists of a reef sequence with a thickness of 873.55 m and a recovery ratio of >70%, and the underlying volcanic basement with a thickness of 55.20 m (Zhang et al., 2018, 2019). The lithologic characteristics and mineralogy were examined by microscopic observation of 300 thin sections under a polarizing microscope. X-ray diffraction (XRD) analysis was also applied to determine the mineralogic composition and diagenetic changes within the samples. Brief lithologic descriptions were conducted by detailed observation of the cuttings during drilling and by selected thin section examination under microscopes in the Guangxi Key Laboratory on the Study of Coral Reefs in the South China Sea, Guangxi University.

Geochemical Measurement of Sr and Mn Contents, and Carbon and Oxygen Isotopes

In total, 875 representative coral, coralline algal, and bulk matrix sediment samples were collected at 1 m sampling intervals and extracted using a dental drill, followed by powdering in an agate mortar. The obviously weathered coats were avoided by visual inspection. The Sr and Mn contents were measured using a Thermo Fisher inductively coupled plasma–mass spectrometer (ICP-MS), and the results are reported in parts per million (ppm). For carbon and oxygen isotope measurements, powdered

samples were reacted with 100% H_3PO_4 at 75 °C in an automated carbonate device to extract CO_2. The $\delta^{18}O$ analyses of all bulk carbonate samples were carried out on a Finnigan MAT-253 stable isotope mass spectrometer attached to a Fairbanks carbonate preparation device. The isotopic ratios are reported in the per mil (‰) convention normalized to Vienna Peedee belemnite (VPDB) using the GBW04405 standard ($\delta^{13}C = 0.57‰$, $\delta^{18}O = -8.49‰$). Multiple measurements ($n = 15$) of this standard yielded a standard deviation of 0.03% for $\delta^{13}C$ and 0.08% for $\delta^{18}O$. Both the Sr and Mn contents and $\delta^{18}O$ measurements were completed at the Coral Reef Research Center of China, Guangxi University.

$^{87}Sr/^{86}Sr$ Measurements

For $^{87}Sr/^{86}Sr$ dating, 100 samples were selected from the previous 875 samples at intervals of 10 m throughout the whole core and 5 m around the lithological boundaries. Further sample preparation and measurements were carried out at the Radiogenic Isotope Facility, University of Queensland, Australia. For the Sr isotope samples, identifiable weathered crusts and diagenetic alteration were thoroughly removed, and then samples were briefly leached with dilute acetic acid before being further dissolved in test tubes overnight in acetic acid. After digestion, the solutions were centrifuged at 4000 rpm for 15 min, and supernates were transferred to precleaned Teflon beakers and dried on a hotplate in a high-efficiency particulate air (HEPA)–filtered ultra-clean environment. Upon dryness, the samples were redissolved in 2 N HNO_3, and Sr was separated using Sr-Spec resin (see Wei et al., 2014). The Sr isotope compositions were measured on a Nu Plasma high-resolution (HR) multicollector ICP-MS with the SRM-987 standard being measured as a drift monitor before and after every five samples. Sr isotope data for both SRM-987 and samples were corrected exponentially for mass fractionation by normalizing to $^{86}Sr/^{88}Sr = 0.1194$. Then, the fractionation-corrected $^{87}Sr/^{86}Sr$ ratios of the samples were further corrected for long-term drift using a polynomial fit through the NIST-987 measurements by normalizing to NIST-987 $^{87}Sr/^{86}Sr = 0.710249$. This standard-sample bracketing method allowed for mass bias in the plasma (which cannot be fully accounted for by the empirical exponential mass fractionation law) to be fully corrected. About 10% of the samples were measured in replicate for quality control. The corrected $^{87}Sr/^{86}Sr$ ratios were projected on the standard age profile of the LOWESS lookup table, which consists of the upper, mean, and lower curves (see McArthur et al., 2001). The mean age is the point of the mean isotopic ratio

on the mean age-ratio curve. The youngest and oldest ages correspond to the mean ± 2σ on the lower curve and upper curve, respectively.

Paleomagnetic Measurements

The sampling intervals varied between 5 and 10 m, depending primarily on the lithology. Paleomagnetic samples were taken by drilling into the core on the top, flat surface of each core section downward with a 2.54-cm-diameter circular diamond laser-positioning drill. The recovered plugs were typically 4 cm long or more. Then, each long plug was cut into two short plugs to fit the size of the sample holder. Our sampling strategy was to collect at least one or two samples per core section or each sampling point. In total, 111 paleomagnetic samples were used during measurement. All of the oriented subsamples were subjected to stepwise alternating field (AF) demagnetization using a 2G-755R cryogenic magnetometer. The natural remanent magnetization (NRM) was measured and demagnetized at 5 mT steps from 0 to 50 mT and then 10 mT steps up to 100 mT. The average inclination of the characteristic remanent magnetization (ChRM) and α_{95} values were computed using AF demagnetization steps following the removal of viscous components. The specimens were eliminated if the ChRM directions could not be ascertained due to ambiguous or noisy orthogonal demagnetization diagrams or extremely weak or unstable magnetization. Those samples that could be linearly fitted toward the origin with mean angular deviation (MAD) <15 degrees during certain demagnetization steps were considered to have a relatively stable component. The demagnetization data were plotted on orthogonal diagrams (Zijderveld, 1967), and the paleo-inclinations of NRM values were determined with principal component analysis (PCA; Kirschvink, 1980). The rotation due to the drilling operation does not permit the cores to be oriented with respect to magnetic north and restricted the paleomagnetic determinations to the vertical component, i.e., paleo-inclination. The paleomagnetic measurements were completed in the paleomagnetism dating laboratory of the South China Sea Institute of Oceanology, Chinese Academy of Sciences, Guangzhou, China.

RESULTS

Lithologic Characteristics and Stratigraphic Division

The reef sequence of CK2 is dominated by different types of limestone and various degrees of dolomite (Fig. 2A). Overall, the stratigraphic units were divided into five parts based
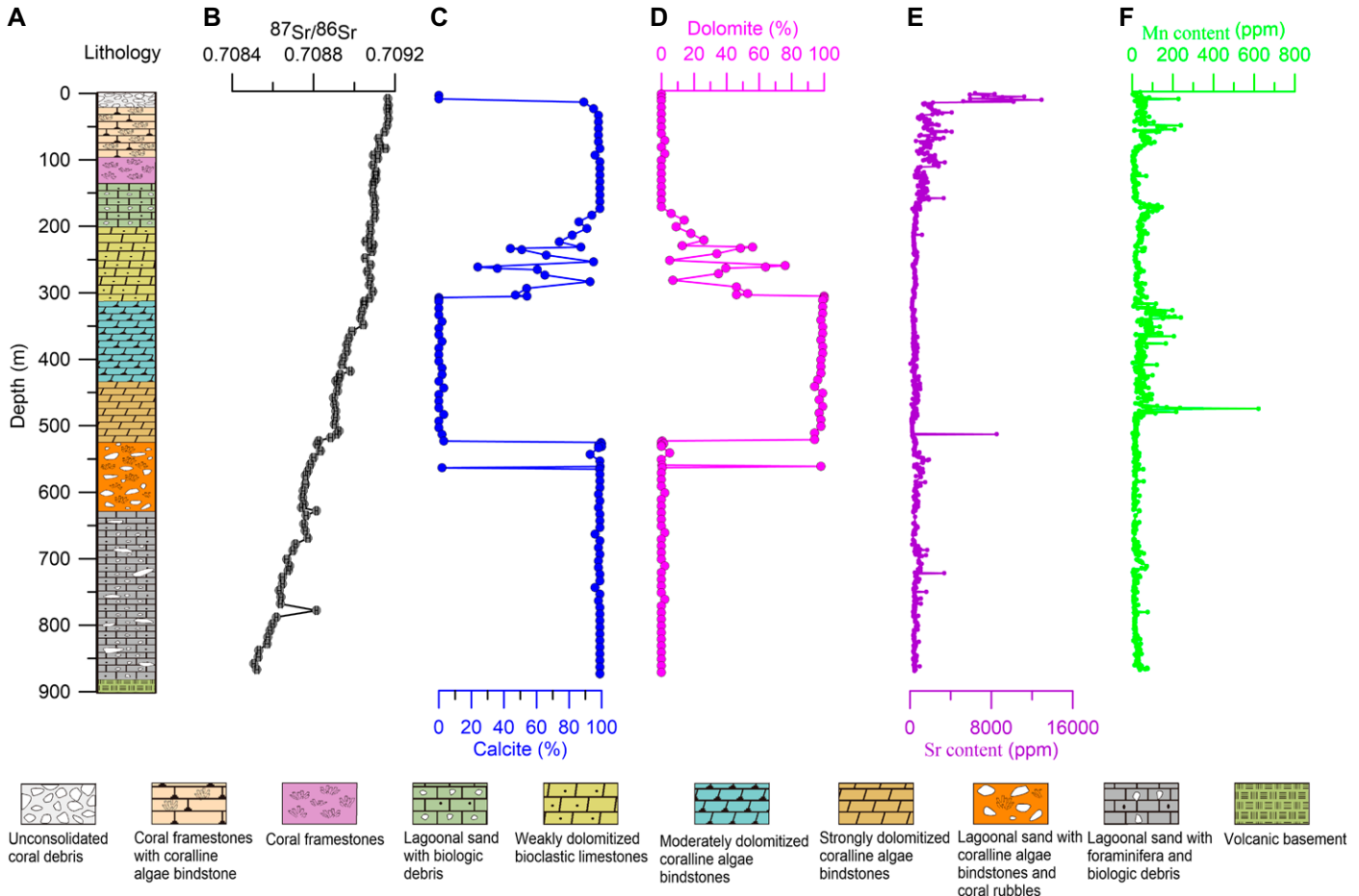
Figure 2. Results from well CK2: (A) lithology, (B) Sr isotope ratios, (C–D) X-ray diffraction (XRD), (E) Sr contents, and (F) Mn contents.

on the lithologic composition and sedimentary characteristics. Part 1 (873.55–522.00 m) is composed of lagoonal sediments with differences in the lower and upper sections. The lower section (873.55–630.74 m) is characterized by thick-bedded to massive lagoon sands, including coral fragments, foraminifera fossils, and other biologic debris, and the upper section (630.74–522.00 m) is characterized by coralline algae bindstones and coral rubble, implying a lagoon slope environment. Part 2 (522.00–312.50 m) is composed of strongly dolomitized coralline algae bindstones in the lower part (522.00–435.00 m) and moderately dolomitized coralline algae bindstones in the upper part (435.00–312.50 m), suggesting a reef crest environment. Part 3 (312.50–132.00 m) is characterized by weakly dolomitized bioclastic limestones containing abundant benthic/planktonic foraminifera and coralline algae in the lower part (312.50–230.00 m) and white to gray bioclastic limestone interbedded with coral rubble in the upper part (230.00–132.00 m). Part 4 (132.00–21.40 m) is composed of coral framestones with some coralline

algae bindstones, suggesting a reef flat to reef crest environment. Part 5 (21.40–0 m) is composed of an unconsolidated mixture of coral debris that has not undergone diagenesis.

Thin section analysis revealed evidence of weak dolomitization in the 230.00–320.00 m section, moderate dolomitization in the 320.00–430.00 m section, and strong dolomitization in the 430.00–520.00 m section. However, excellent skeletal preservation of fossil coral, coralline algal crusts, and other bioclastics could still be identified at these depths. XRD analysis showed that most samples are composed of aragonite, low-magnesium calcite, or high-magnesium calcite and dolomite (Figs. 2C and 2D). The mineral composition of the 320.00–520.00 m section showed a higher dolomite content than the other parts, in accordance with the thin section results.

Geochemical Results of Sr and Mn Content and Oxygen Isotope Analysis

The Sr and Mn contents (Figs. 2E and 2F) were obtained for further detection of the degree

of diagenetic alteration, and they are discussed in the following sections. The Sr contents can be divided into three classes (Fig. 2E): (1) The Sr content of the upper part above 14.00 m is the highest up to 12936.48 ppm at 11.00 m. (2) The Sr content between 15.00 and 110.00 m fluctuates between 574.91 and 4096.84 ppm. (3) The Sr content below 110.00 m is lower than 1854.90 ppm for most samples, although some samples have abnormally high values (for instance, the Sr content of the sample at 514.00 m is 8534.95 ppm). The Mn content of most samples is lower than 100 ppm, with exceptions at 11.00 m, 51.00–57.00 m, 171.00–181.00 m, and 319.00–484.00 m (Fig. 2F). The highest Mn content is 620.05 ppm at 477.00 m.

The $\delta^{18}O$ values of these bulk carbonate samples vary from –8‰ to 5‰ (average 2.24‰), as illustrated in Figure 3B. For part 1 (873.55–522.00 m), the $\delta^{18}O$ values range from –7.46‰ to 0.14‰ (average –4.14 ‰). The $\delta^{18}O$ values of part 2 (522.00–312.50 m) range from 1.96‰ to 4.31‰ (average 3.35‰). Similarly, the $\delta^{18}O$ values of part 3 (312.50–132.00 m) range from 0.84‰ to 4.54‰ (average 1.40‰), and the
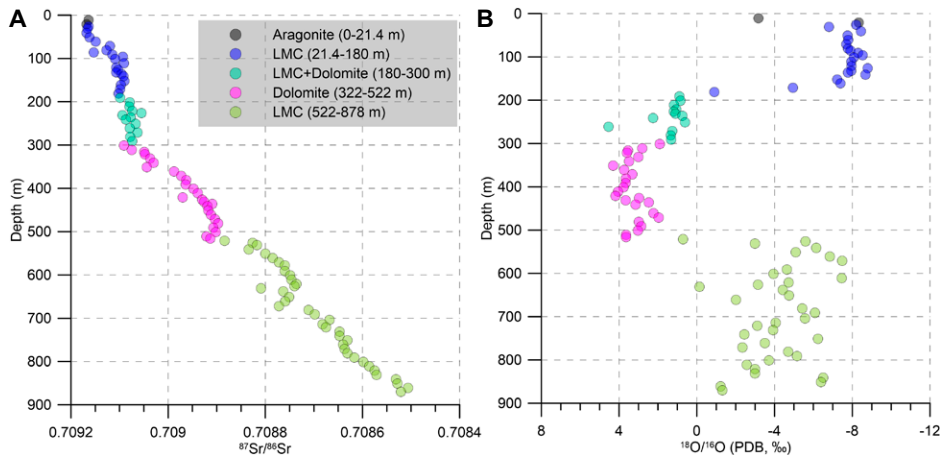
Figure 3. (A) $^{87}Sr/^{86}Sr$ and (B) $^{18}O/^{16}O$ values with depth for all bulk carbonate samples. The samples can be divided into five types according the X-ray diffraction (XRD) results (see Figs. 2C and 2D), where different types of bulk samples are illustrated using different-colored filled circles. LMC—low-magnesium calcite; PDB—Peedee belemnite.

$\delta^{18}O$ values of part 4 (132.00–21.40 m) range from –6.81‰ to –8.79‰ (average –8.00‰). The $\delta^{18}O$ values of two samples from part 5 are –3.17‰ and –8.33‰, respectively. The $\delta^{18}O$ values of partially dolomitized limestone or dolostone samples, ranging from 0 to 5‰ (average 2.63‰), is much larger than those of low-magnesium calcite and aragonite samples (average –5.38‰).

$^{87}Sr/^{86}Sr$ Results

The $^{87}Sr/^{86}Sr$ data are plotted against their collection depths in Figure 3A. The minimum value of $^{87}Sr/^{86}Sr$ is 0.708506 at a depth of 861.00 m, and the maximum value is 0.709168 at a depth of 21.00 m. The $^{87}Sr/^{86}Sr$ values show a general monotonic increase with decreasing depths, with the exception of some abnormally high outliers within the 620.00–670.00 m (values between 0.708751 and 0.708809), 430.00–520.00 m (values between 0.708897 and 0.708970), and 230.00–300.00 m (values between 0.709063 and 0.706091) intervals. Considering that reef carbonates are vulnerable to diagenetic alteration by a variety of pore fluids (e.g., dolomitization) during their diagenetic history, the bulk rock always contains impurities that affect the measured $^{87}Sr/^{86}Sr$ values. The effect of diagenetic alteration on the $^{87}Sr/^{86}Sr$ values is observed in the dolomitized sections at the depths of 230.00–320.00 m and 430.00–520.00 m.

The standard calibrated $^{87}Sr/^{86}Sr$ ratios show a general monotonic increase with decreasing depth or age since 40 Ma, and many linear segments are separated by intervals during which the rate of change in the $^{87}Sr/^{86}Sr$ values with time changed (McArthur et al., 2001). The long-term trend shows that the $^{87}Sr/^{86}Sr$ ratios of well CK2 increase monotonically with decreasing depth, indicating that the $^{87}Sr/^{86}Sr$ ratios evolved with the same behavior and represent the original seawater $^{87}Sr/^{86}Sr$ composition, although various degrees of diagenetic alteration occurred at different intervals.

Paleomagnetic Results

Paleo-inclinations were evaluated and calculated from the vertical projection in orthogonal diagrams. Figures 4A–4D show four examples of samples with characteristic reversed and normal field directions preserved. The magnetic directions below 30 mT are highly variable for most samples. This is interpreted to be a viscous magnetic overprint of the samples acquired after deposition. During 30 and 80 mT AF demagnetization, most samples reveal a characteristic component trending toward the origin, and the path toward the origin shows relative stability, with a highly linear trend (low MAD). These samples are typically better defined by line fits with MAD values <15 degrees (Fig. 4F). We infer that this direction represents a primary magnetization, based on correlation of the acquired polarity zones with the geomagnetic polarity time scale (Ogg, 2012) according to the numerical ages of $^{87}Sr/^{86}Sr$ ratios as discussed in the following section. For our samples, an up inclination corresponds to reversed polarity, whereas a down inclination corresponds to normal polarity. The polarity intervals were defined by grouping adjacent sample polarities and matching them to the polarity chrons and subchrons of the geomagnetic polarity time scale (Ogg, 2012). At least two to three successive ChRM directions were required to define polarity zones, consider-

ing the weak ChRM of the carbonates. Finally, the changes in the paleo-inclinations with depth are illustrated in Figure 4E.

DISCUSSION

Effect of Diagenetic Alteration on $^{87}Sr/^{86}Sr$ Results

The use of Sr isotopes for dating requires samples that contain the original Sr isotope ratios of contemporaneous seawater at the time of deposition. For dating carbonates, Sr isotope dating also requires that subsequent diagenetic alteration has not significantly altered the original ratios after deposition. Younger seawater circulating around the atoll margin carbonates would have had higher $^{87}Sr/^{86}Sr$ ratios than the original deposited carbonate. Therefore, diagenetic contamination would cause a higher apparent Sr isotope ratio and a younger apparent age than the true depositional ratio and age (Vahrenkamp et al., 1988; Saller and Koepnick, 1990). Furthermore, Scasso and Kiessling (2001) suggested that the meteoric diagenesis of carbonate potentially produces older-than-actual ages in environments where fluids could interact with basaltic rock, while later-stage marine diagenesis has the potential to decrease the apparent age of the samples. Hence, careful inspection of diagenesis is necessary, and the $^{87}Sr/^{86}Sr$ samples should be carefully checked for minimal diagenetic alteration.

The methods and criteria used to judge the degree of diagenetic alteration of bulk carbonate are similar to those used for fossil materials and include petrographic and cathodoluminescence microscopy, and trace-element and stable isotope ($\delta^{18}O$ and $\delta^{13}C$) analysis (Veizer, 1989; Derry et al., 1992; Azmy et al., 2009). The $\delta^{13}C$ result is not discussed here because the $\delta^{13}C$ values of the diagenetic carbonate should not be significantly different than the $\delta^{13}C$ values of the original sediments (Hayes et al., 1999; Bachan et al., 2012). Additionally, Sr concentration ([Sr]) and/or Mn/Sr or Sr/Mn ratios are used to screen bulk-rock samples and to delineate fields of least-altered samples (Burke et al., 1982; Halverson et al., 2007; Derry et al., 1992; Montañez et al., 1996; Young et al., 2009). In the absence of well-preserved fossil materials, the best way is to use multiple methods or criteria together to assess alteration.

Preservation of Depositional Ratios

For the corals and coralline algae, most of the deposited carbonate samples were mainly high-magnesium calcite when deposited. For CK2, the bulk-rock samples (except at 200–522 m
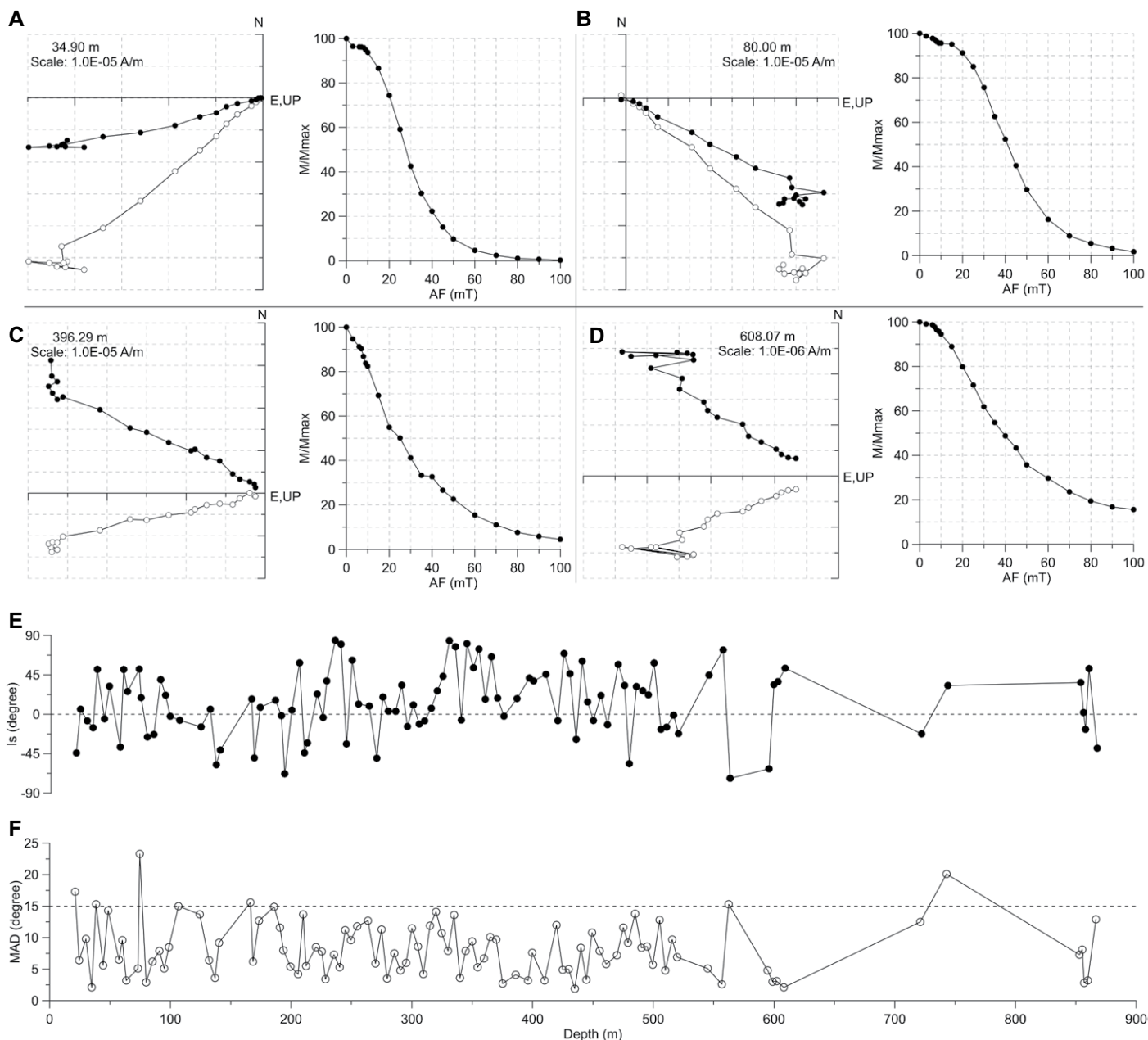
Figure 4. (A–D) Representative alternating field (AF) demagnetization plots of natural remanent magnetization (NRM) for normal and reverse polarity samples. M/M$_{max}$ is the ratio of measured remanent magnetization at different levels to the maximum magnetization at zero demagnetization. White dots correspond to the vertical plane, and black dots correspond to projection on the horizontal plane. Inclinations shown as circles on the vertical projections represent levels of stepwise AF demagnetization in units of millitesla (mT). (E) Changes of inclinations (Is) of all samples vs. depth. (F) Changes of mean angular deviation (MAD) vs. depth.

depth) were converted to low-magnesium calcite, and the samples at a depth of 200–522 m have the highest magnesium (Mg) concentrations, suggesting the occurrence of diagenetic alteration and conversion from calcite to dolomite (Figs. 2C and 2D). Overall, the lithologic, petrologic, and geochemical results together suggest the occurrence of various degrees of diagenetic alteration. All depositional carbonate samples were divided according to calcite

and dolomite content into four groups, as described below.

The first group (0–21.4 m) exhibits no diagenetic alteration and contains depositional high-magnesium calcite and aragonite (Figs. 2A, 2C, and 2D). This group should record the depositional Sr isotope ratio of the contemporaneous seawater.

The second group (21.4–180 m and 522–878 m) mainly consists of depositional low-

magnesium calcite. For this group, the Mn/Sr ratios (ranging from 0.01 to 0.5; Fig. 5C) are much lower than 2–3 (Kaufman et al., 1992, 1993). For most of our samples, the Sr contents are much higher than ~200 ppm or 300 ppm (Fig. 5B), as proposed by Derry et al. (1989) and Edwards et al. (2015), and the contents of Mn (Fig. 4B) are far lower than ~250 ppm, as proposed by Korte et al. (2003). Quinn et al. (1991) and Wilson et al. (1998) proposed that
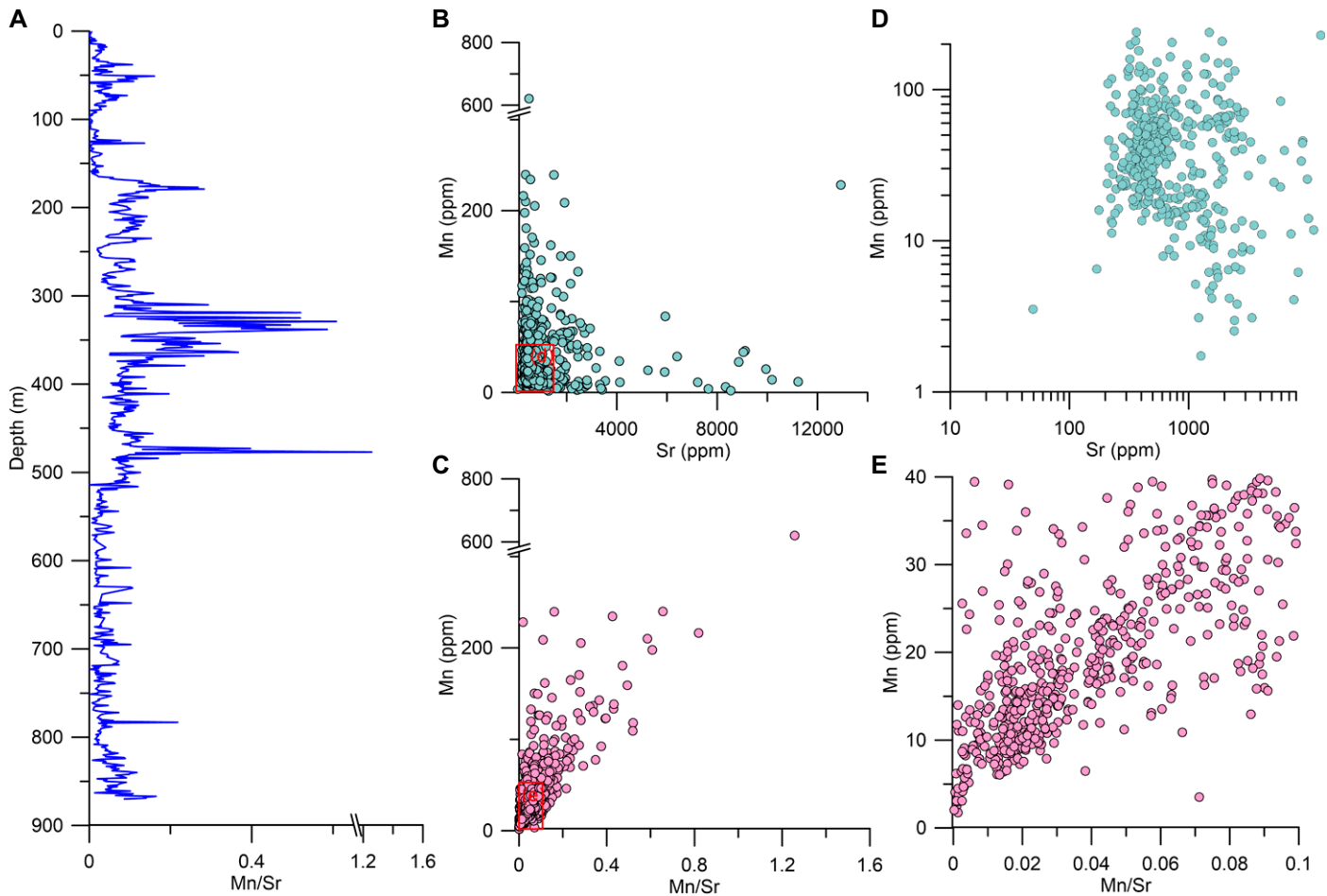
Figure 5. (A) Changes in the Mn/Sr ratio with depth, (B) correlation between Mn content and Sr content, and (C) Mn/Sr ratio vs. Mn content. Inset (red box) in B is enlarged in D, and inset (red box) in C is enlarged in E.

both closed-system and open-system meteoric diagenesis will result in the preservation of the original $^{87}Sr/^{86}Sr$ ratio during diagenetic alteration of aragonite to low-Mg calcite, except where there is a significant input of Sr from an additional source having a markedly different Sr isotopic composition. The reason is that Sr in pore water and resident bulk carbonate is rarely in isotope equilibrium, suggesting that pore water may carry Sr either more or less radiogenic than resident Sr (Gieskes et al., 1986). In our data set, there are no apparent correlations between the $^{87}Sr/^{86}Sr$ and Sr content (Fig. 6B), suggesting that the Sr content was not the controlling factor in the variation of $^{87}Sr/^{86}Sr$. There also is no clear correlation between $^{87}Sr/^{86}Sr$ and $\delta^{18}O$ (Fig. 6A). In addition, the increase in the Sr isotope ratios, corresponding to a consistent $^{87}Sr/^{86}Sr$ trend from the Miocene to present (McArthur et al., 2001), further suggests that the process responsible for converting high-magnesium calcite to low-magnesium calcite did not significantly change the Sr isotope ratios in this second group of samples.

For the third group (180–300 m), the XRD data show the coexistence of calcite and dolomite, and two minimum values of low-magnesium calcite content appear at 240 m and 260 m, respectively (Figs. 2C and 2D). The degree of diagenetic alteration increases downward through this section; however, the $^{87}Sr/^{86}Sr$ ratios keep decreasing slowly, suggesting the original seawater ratios may be still retained in some samples with low $^{87}Sr/^{86}Sr$ values. No apparent correlation between $^{87}Sr/^{86}Sr$ and Sr content, $^{87}Sr/^{86}Sr$, or $\delta^{18}O$ is observed (Fig. 6). The Sr contents of all samples but one is higher than 300 ppm and agree with the criteria proposed by Edwards et al. (2015). The Mn/Sr ratios (between 0.05 and 0.48; Fig. 5C) are also much lower than 2–3, and the Mn contents are lower than 250 ppm. All these lines of evidence suggest that the original depositional Sr isotope ratios may be retained in the third group of samples, although some bulk carbonate may have been dolomitized. However, fluctuations in the $^{87}Sr/^{86}Sr$ ratios with decreasing depth strongly suggest that diagenetic alteration has

altered the original Sr isotope ratios to some extent. Our finding further supports the findings of Ludwig et al. (1988), in which they showed that diagenetic alteration in freshwater did not alter the original Sr isotope ratios in the Miocene to Pleistocene carbonate on Enewetak Atoll. Their reason states that the calcite that precipitated in freshwater lenses was derived from adjacent depositional carbonate with the Sr isotope ratio of seawater at the time of deposition (Ludwig et al., 1988). For CK2, nonetheless, we speculate that multiple instances of major introductions of foreign Sr could have resulted in some samples being more radiogenic than the overlying/underlying samples. The fact that some samples are out of stratigraphic order and the consequent fluctuations of the $^{87}Sr/^{86}Sr$ ratios upward suggest that primary or near-primary seawater ratios were possibly retained in some bulk carbonate samples, although diagenetic alteration occurred.

The fourth group (300–522 m) is almost completely composed of calcian dolomite with only minimal amounts of low-magnesium
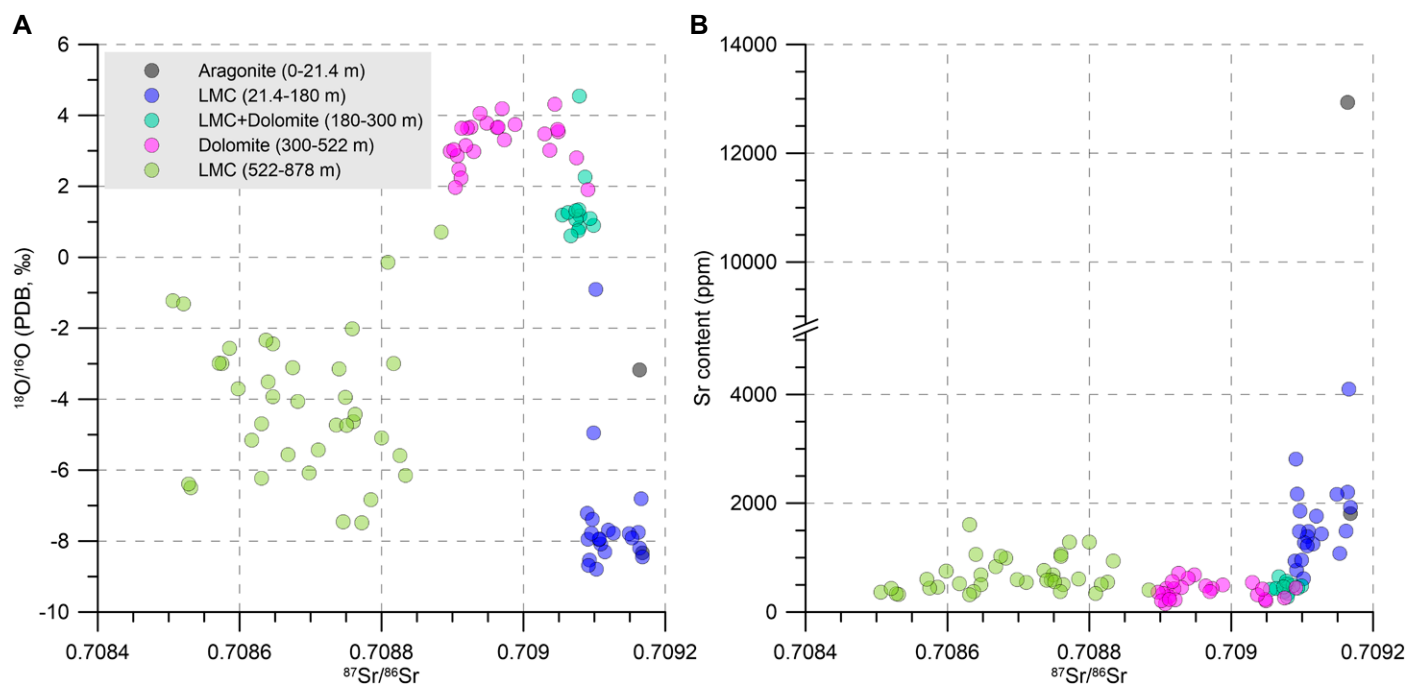
Figure 6. (A) Plot of $^{87}Sr/^{86}Sr$ vs. $^{18}O/^{16}O$, and (B) plot of $^{87}Sr/^{86}Sr$ vs. Sr content of bulk carbonate samples. LMC—low-magnesium calcite; PDB—Peedee belemnite.

calcite (Fig. 2A). The detailed evidence and discussion of these dolostones were given in Wang et al. (2018). The Sr and Mn contents are higher than 200 ppm and lower than 250 ppm, respectively, except for a few abnormal values (Fig. 5B). The Mn/Sr ratios fall between 0 and 1.3 (Fig. 5C), which is lower than the range of 2–3 proposed by Kaufman et al. (1992, 1993). No apparent correlation between $^{87}Sr/^{86}Sr$ and Sr content is observed, and the relationship between $^{87}Sr/^{86}Sr$ and $\delta^{18}O$ is also not obvious (Fig. 6). Furthermore, the Sr isotope ratios increase overall in accordance with the continued increase in the $^{87}Sr/^{86}Sr$ curves of McArthur et al. (2001). All these observations suggest that the diagenetic alteration process or the process responsible for converting low-magnesium calcite to dolomite did not significantly alter the depositional Sr isotope ratios in this group of samples. This findings is also consistent with previous studies, which found that some dolomite samples with low Sr content appear to preserve $^{87}Sr/^{86}Sr_{seawater}$ (Li et al., 2011; Liu et al., 2013). Li et al. (2011) found that some dolomitic rock components may retain a near-primary seawater $^{87}Sr/^{86}Sr$ composition. Liu et al. (2013) interpreted the minimum $^{87}Sr/^{86}Sr$ ratios in dolostones to represent Sr isotope compositions of penecontemporaneous seawater, similar to values for high-Sr limestones under- and overlying dolostones around the world.

Age Profile of Strontium Isotope Stratigraphy

The selection of relatively reliable Sr isotope ratios was completed following three criteria: (1) Sr isotope ratios must monotonically increase with decreasing depth, corresponding to the general increasing trend of Sr evolution from the Miocene to present. (2) Abnormally high or low Sr isotope ratios were rejected because they are out of stratigraphic order. (3) Lower Sr isotope ratios were selected for those samples that potentially underwent diagenetic alteration because the younger seawater would have higher $^{87}Sr/^{86}Sr$ ratios than the originally deposited carbonate. Ultimately, 58 reliable $^{87}Sr/^{86}Sr$ data points were selected and converted to numerical ages (Table 1) according to the standard calibrated $^{87}Sr/^{86}Sr$ curve of McArthur et al. (2001); these are shown in Figure 7. The $^{87}Sr/^{86}Sr$ ratio ranges from 0.708506 to 0.709168, corresponding to ages from 19.20 Ma to 0.35 Ma. The age corresponding to the bottom at 873.55 m is 19.60 Ma based on the extrapolation of the sedimentation rate, suggesting that the atoll started to form at that time.

Effect of Diagenetic Alteration and Sedimentation Rate on Paleomagnetic Results

Paleomagnetic dating has been successfully applied to carbonate and has proven to

be an effective and important approach for providing reliable age control and estimating the average sediment accumulation rate (SAR) between magnetic reversal boundaries (Lu et al., 1996; Ménabréaz et al., 2010). However, many factors, such as diagenetic alteration, sedimentation hiatus, and sedimentation rate changes, can distort the shapes of polarity zones. Here, we focus our discussion on these three aspects.

No systematic changes or trends were found in the paleo-inclination series (Fig. 4) for both sections that exhibited moderate diagenetic alteration or distinctive diagenetic alteration. For instance, the documentation of polarities across the dolomitized zones (230.00–520.00 m) with no significant changes suggested that diagenesis has not impaired the primary polarity pattern. Therefore, the influence of diagenetic alteration can be ignored, although further study is still needed.

The occurrence of a sedimentation hiatus can lead to missing polarity zones, and a change in SAR can lead to extended or shortened magnetozones. At least 10 potential hiatuses in CK2 were revealed and complicated the correlation of the observed polarity zones to the global geomagnetic polarity time scale (GPTS). The SAR changes with depth were calculated by using numerical age controls (Fig. 8). Abrupt increases in SAR occurred at depths of 101.00–121.00 m, 690.00–714.00 m, and

TABLE 1. SELECTED SR SAMPLES FROM WELL CK2 (SOUTH CHINA SEA) AND THE OBTAINED AGES

| Sample no.	Core depth (m)	$^{87}Sr/^{86}Sr$	2σ	Minimum age (Ma)	Mean age (Ma)	Maximum age (Ma)
CK2-E21	21	0.709168	0.000011	0.162	0.212	0.268
CK2-E31	31	0.709166	0.00001	0.228	0.282	0.342
CK2-E51	51	0.709162	0.00001	0.366	0.427	0.52
CK2-E61	61	0.709149	0.00001	0.655	0.738	0.823
CK2-E81	81	0.709127	0.000012	1.139	1.181	1.228
CK2-E91	91	0.709115	0.000012	1.276	1.324	1.368
CK2-E101	101	0.709109	0.000013	1.35	1.396	1.448
CK2-E121	121	0.709107	0.000012	1.375	1.423	1.483
CK2-E126	126	0.709103	0.000012	1.425	1.485	1.565
CK2-E136	136	0.709096	0.000009	1.552	1.657	1.768
CK2-E141	141	0.709092	0.000011	1.671	1.776	1.886
CK2-E152	152	0.70909	0.000012	1.727	1.837	1.964
CK2-E201	201	0.709079	0.000012	2.1	2.21	2.32
CK2-E221	221	0.709074	0.000012	2.26	2.37	2.51
CK2-E251	251	0.709067	0.000011	2.52	2.73	3.38
CK2-E271	271	0.709063	0.000011	2.68	3.38	3.68
CK2-E316	316	0.709049	0.000009	4.15	4.45	4.68
CK2-E321	321	0.709048	0.000014	4.23	4.52	4.73
CK2-E331	331	0.709037	0.000012	4.89	5	5.09
CK2-E341	341	0.70903	0.000011	5.1	5.18	5.28
CK2-E361	361	0.708988	0.000013	5.94	5.98	6.02
CK2-E371	371	0.708973	0.000012	6.12	6.18	6.27
CK2-E381	381	0.708963	0.000011	6.37	6.5	6.64
CK2-E401	401	0.708948	0.00001	6.77	7.03	7.35
CK2-E411	411	0.708939	0.000012	7.1	7.39	7.95
CK2-E426	426	0.70893	0.00001	7.42	8.1	8.58
CK2-E431	431	0.708926	0.000012	7.57	8.38	8.78
CK2-E441	441	0.708919	0.000009	8.31	8.74	9.07
CK2-E451	451	0.708917	0.000008	8.43	8.83	9.16
CK2-E461	461	0.708912	0.00001	8.69	9.04	9.39
CK2-E471	471	0.708904	0.000009	9.06	9.38	9.71
CK2-E481	481	0.708897	0.000008	9.33	9.67	10
CK2-E521	521	0.708884	0.00001	9.88	10.19	10.45
CK2-E526	526	0.708826	0.000009	12.07	12.55	12.89
CK2-E531	531	0.708817	0.00001	12.66	12.98	13.31
CK2-E551	551	0.7088	0.00001	13.42	14.03	14.55
CK2-E561	561	0.708785	0.000012	14.52	14.87	15.13
CK2-E571	571	0.708772	0.000011	15.08	15.31	15.51
CK2-E578	578	0.70876	0.00001	15.45	15.64	15.82
CK2-E601	601	0.708749	0.000009	15.73	15.9	16.07
CK2-E611	611	0.708746	0.000009	15.8	15.97	16.14
CK2-E626	626	0.70874	0.000008	15.93	16.1	16.26
CK2-E681	681	0.708711	0.000008	16.5	16.62	16.73
CK2-E691	691	0.708698	0.000009	16.71	16.82	16.92
CK2-E714	714	0.708682	0.000009	16.93	17.03	17.12
CK2-E721	721	0.708675	0.000009	17.02	17.12	17.2
CK2-E731	731	0.708647	0.00001	17.36	17.44	17.52
CK2-E761	761	0.70864	0.00001	17.44	17.51	17.59
CK2-E771	771	0.708637	0.000009	17.47	17.55	17.62
CK2-E781	781	0.708631	0.000011	17.53	17.61	17.68
CK2-E791	791	0.708617	0.000008	17.68	17.76	17.85
CK2-E801	801	0.708598	0.000009	17.9	17.98	18.06
CK2-E811	811	0.708586	0.00001	18.03	18.12	18.2
CK2-E821	821	0.708575	0.000009	18.16	18.24	18.34
CK2-E831	831	0.708571	0.000011	18.2	18.29	18.39
CK2-E841	841	0.708531	0.000008	18.73	18.83	18.93
CK2-E851	851	0.708528	0.000011	18.77	18.88	18.98
CK2-E861	861	0.708506	0.000008	19.1	19.2	19.31

Paleomagnetic Age Profile

Ten normal polarity (N1–N10) and eight reversed polarity (R1–R8) magnetozones were identified (Fig. 9). Based on the numerical age controls, the boundaries of the Pleistocene-Pliocene and Pliocene-Miocene are located at 237.00 m and 364.00 m in the CK2 core, respectively. During the Miocene, the boundaries of the late Miocene to mid-Miocene and the mid-Miocene to early Miocene are further located at 522.00 m and 611.00 m, respectively. As shown in Figure 5, at the top of the CK2, local magnetozone N1 (at a depth range of 0–74.00 m) should correlate to the chrons C1n to C1r.1n of the GPTS, considering that the numerical ages at 57.00 m and 74.00 m are 0.61 Ma and 1.026 Ma, respectively. The magnetozone R2 between 107.00 and 166.00 m is characterized by a distinctive reversal with a potential normal polarity, and this pattern appears to be correlated with chrons C1r to C2n of the GPTS. Magnetozones N3–N5 between 166.00 and 295.00 m are dominated by three normal and two reversed polarity zones, and some potential short events occur in N5 and N6. The distinctively normal polarities appear to correlate to chrons C2r to C2An.3n of the GPTS. In the middle part of the CK2 core (315.00–444.00 m), magnetozone N6 is characterized by a thick normal polarity zone with several potential reversals. In addition, the numerical ages of $^{87}Sr/^{86}Sr$ at 315.00 m and 444.00 m are 4.43 and 8.767 Ma, respectively. We tentatively correlate magnetozone N6 to chrons C3n.2n to C4An of the GPTS. For N7, the numerical age of $^{87}Sr/^{86}Sr$ at 499.00 m is 9.90 Ma, suggesting that it correlates to C5n.1n of the GPTS. The numerical age of $^{87}Sr/^{86}Sr$ of the upper limit (602.00 m) of magnetozone N9 is 15.91 Ma; however, no paleo-inclinations were gained between 608.00 and 721.00 m. Therefore, magnetozone N9 is tentatively correlated to C5Cn.1n of the GPTS. Magnetozone N10 is composed of a normal polarity zone with a potential short reverse polarity event. According to the numerical age of $^{87}Sr/^{86}Sr$ at 853.00 m of 18.94 Ma, magnetozone N10 is tentatively correlated to C6n of the GPTS.

Finally, the magnetostratigraphic record was established and correlated with the GPTS using numerical age-control points from $^{87}Sr/^{86}Sr$. On the basis of these correlations and numerical ages, we suggest that the present polarity chronozones extend from chron C6 at 866.60 m to present at the top (Fig. 9). Nonetheless, it should be noted that the magnetostratigraphy is a rough and preliminary correlation, considering the low resolution of sampling and the scarcity of samples in the lower part of the CK2 core. Further detailed correlation is needed if more samples can be acquired in future studies.

731.00–761.00 m, respectively. The distinctively long-polarity reversal between 101.00 and 150.00 m is associated with the abrupt increase in SAR. The SAR at the depth range of 250.00–550.00 m is slower than the SAR of other sections, and the lowest value occurs at a depth of 526.00 m. Hence, the length of the polarity zones of the sections with low SAR may be shorter, and the existence of at least four hiatuses further complicates the correlation to the GPTS. The influences of the hiatus and SAR are not discussed for the section below 600.00 m because few paleo-inclination points were recorded due to unconsolidated lagoon sands, which precluded the acquisition of paleomagnetic samples.
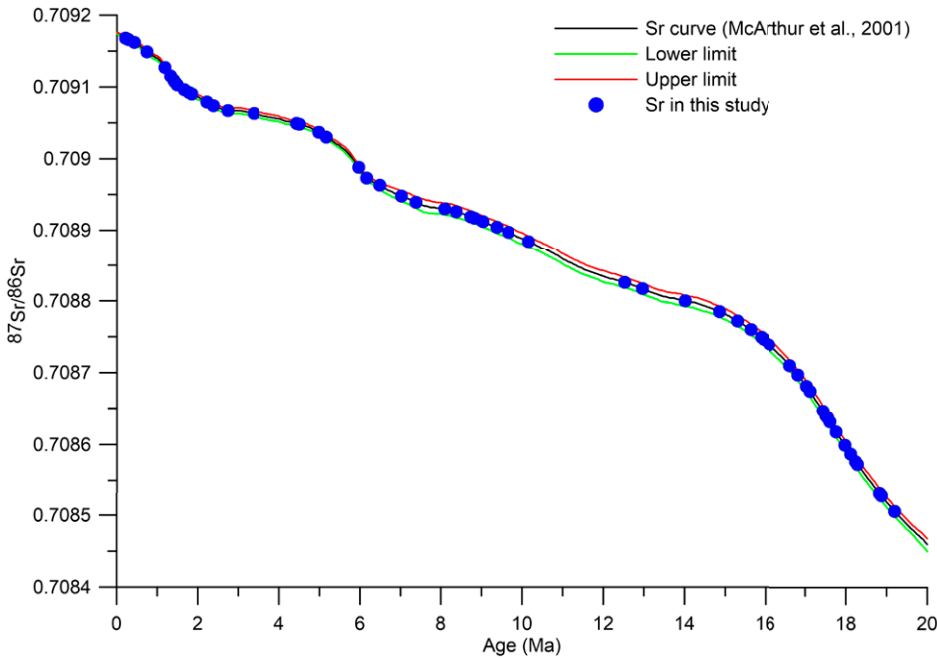
Figure 7. Projection of the selected Sr isotope samples from well CK2 on global standard calibrated Sr curves (McArthur et al., 2001). Lower limit and upper limit of Sr curve (McArthur et al., 2001) are 95% confidence bounds.

Reconstruction of the Evolutionary History Based on New Age Profile

Previous studies suggested that three large-scale drowning events were recorded during the late early Miocene (17.5–13.8 Ma), early late Miocene (10.0–8.2 Ma), and middle to late Pliocene (3.4–3.0 Ma), respectively. The reefs changed from barrier reefs to atoll reefs during the late Pliocene (3.0–2.6 Ma) and Quaternary and became submerged by the end of the Quaternary (Xu et al., 2002). Ma et al. (2011)
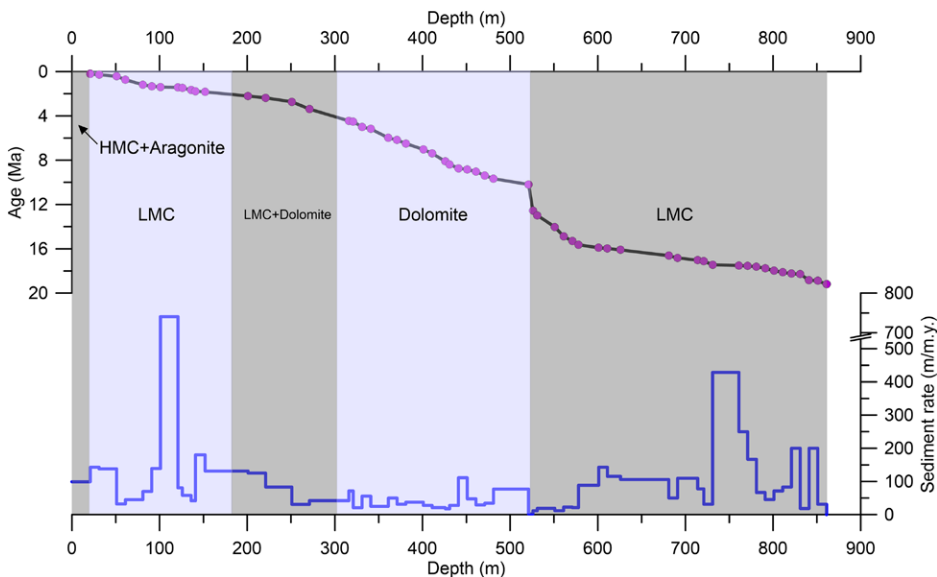
Figure 8. Plot of the ages of the Sr isotope ratios vs. depth (upper) and changes in the sedimentation accumulation rate with depth (lower). Boundaries of the different filled boxes were determined from the X-ray diffraction (XRD) results, and the major mineral components are indicated. LMC—low-magnesium calcite; HMC—high-magnesium calcite.

proposed five stages in the development of the Xisha carbonate platform based on seismic data. Furthermore, according to newly acquired seismic data, Wu et al. (2014, 2016) divided the evolution into four stages: early Miocene initiation (23.3–15.5 Ma), middle Miocene large-scale growth (15.5–10.5 Ma), late Miocene drowning (10.5–5.5 Ma), and Quaternary isolated buildup on topographic highs (2.4–0 Ma). However, no new direct age data were reported, and all these studies were mainly based on biostratigraphy, lithostratigraphy, and seismic data.

In the present study, according to the lithologic analysis, petrologic results, and new chronologic dating, the evolution of Chenhang Island can be reconstructed (Fig. 10) since initiation as follows: (1) initiation phase (19.6–16.26 Ma); (2) development phase (16.26–10.66 Ma); (3) drowned to development phase (10.66–4.36 Ma); (4) drowned to development phase (4.36–1.59 Ma); and (5) development phase to drowned phase (1.59 Ma–present).

During the early Miocene between 19.60 and 16.26 Ma, the thick fine lagoon sands, small coral debris, and/or shell fossils suggest that Chenhang Island experienced rapid subsidence. This rapid subsidence of the basement most likely resulted in the drowning of the Xisha carbonate platform, as supported by the first drowning events (17.5–13.8 Ma) recorded in well Xiyong-1 (Xu et al., 2002) and well 120-CS-1X (Fyhn et al., 2013). The sedimentation rate during 17.44–17.51 Ma (731–761 m) was 428 m/m.y. due to rapid subsidence of the basement, because there is no evidence showing a sharp fall of global sea level or significant change of paleoceanographic conditions. Our results are also verified by the seismic data, which suggest the reefs were typically restricted, with a limited extent on top of the carbonate platforms, dominated by fringing reefs along the margins and/or patch reefs in the tectonically stable area west of the region of the present Xisha Islands (Wu et al., 2014; Shao et al., 2017).

During the early Miocene (19.6–16.26 Ma) period, the reef island started the first development phase. Following ~3 m.y. of lagoon environment, abundant coral debris and coral framestones were preserved from 16.26 Ma to 10.66 Ma in the study area, suggesting that subsidence slowed, and the environment fluctuated between lagoon and lagoon slope. The seismic profiles of this phase are characterized by moderate and low amplitudes and parallel reflections of lagoons, indicating a stable sedimentary environment (Ma et al., 2011; Wu et al., 2014).

From the late Miocene, reefs were drowned during 10.66–8.52 Ma, and the environment then gradually changed to reef crest (8.52–4.36 Ma). The drowning of the reefs is
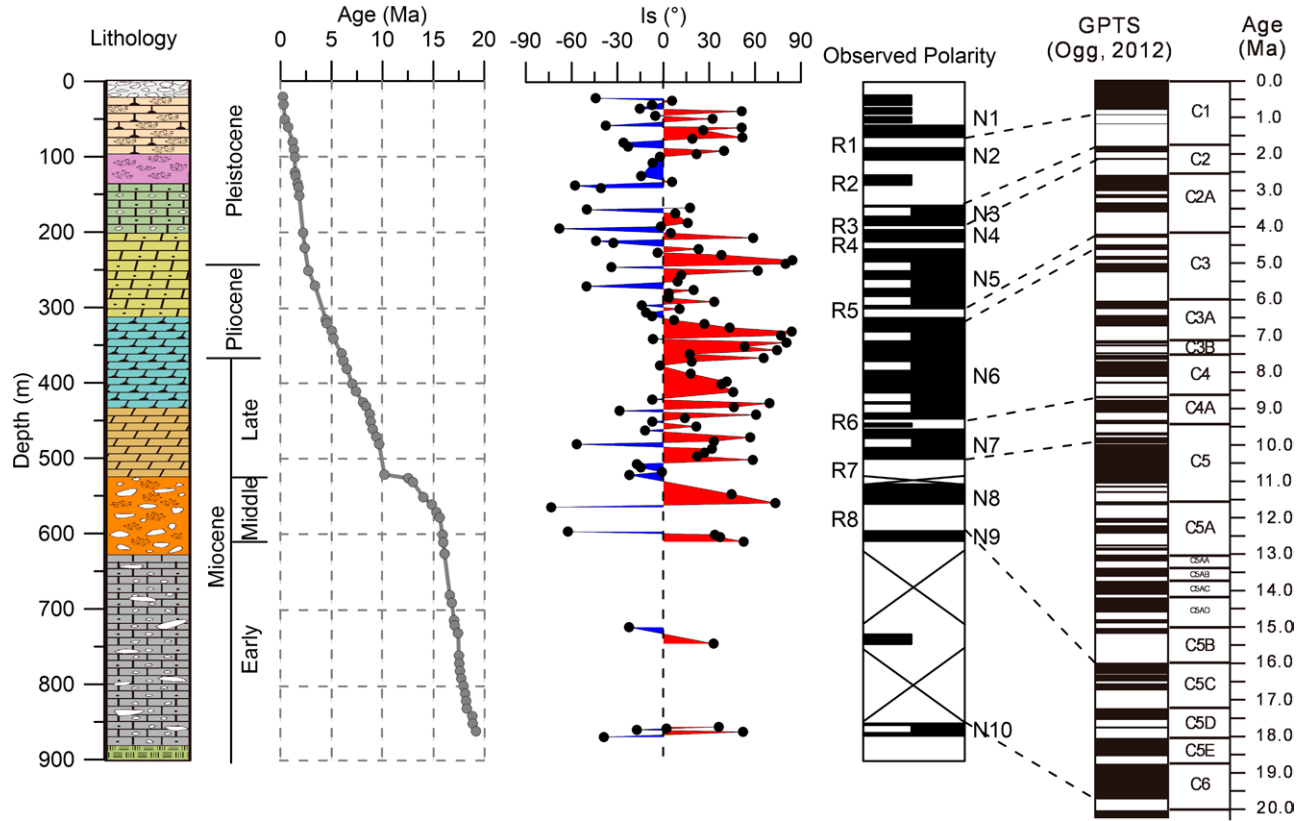
Figure 9. Results of lithostratigraphy, strontium isotope stratigraphy, and magnetostratigraphy from well CK2 and their correlation with the geomagnetic polarity time scale (GPTS; Ogg, 2012). See Figure 2 for lithology legend. Is—inclinations.
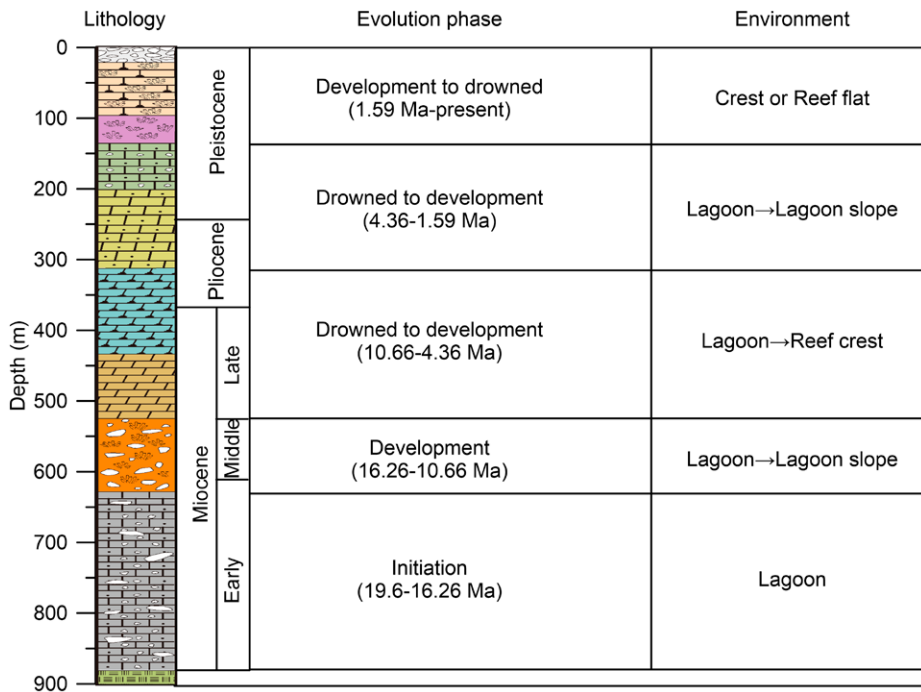

Figure 10. Division of reconstructed evolutionary phases and the interpreted environments of the reef based on the new chronologic framework from the strontium isotope stratigraphy and magnetostratigraphy results in this study.

confirmed in previous well data that show a lagoon developed in the Xuande Islands during this phase (Zhang et al., 1989, 1996) and in well Xiyong-1 (Xu et al., 2002). The next drowned to development phase at 4.36–1.59 Ma suggests that the subsidence potentially accelerated during 4.36–2.48 Ma and became slow again during 2.48–1.59 Ma. The drowning event can be correlated with the last large-scale drowning recorded in well Xiyong-1 (Xu et al., 2002).

Since the early Pleistocene (1.59 Ma), the reef island started drowning again, which has continued to the present. Previous studies suggested that the carbonate platforms on the west Xisha uplift began to drown in the Pliocene due to rapid relative sea-level rise and increasing input of terrestrial siliciclastics (Xu et al., 2002; Clift and Sun, 2006; Fyhn et al., 2013). Isolated carbonate platforms remained on structural highs and transformed into large-scale atoll reefs, which have survived to present (Wu et al., 2014). A very high sedimentation rate during 1.40–1.42 Ma (101–121 m) is observed, which may be related to the rapid subsidence of basement, because the global sea level reached its maximum and has since begun to decline. For CK2, we therefore attribute the development of reef during this phase to the regional structural

highs and the moderate rise in the relative sea level.

In summary, our preliminary age data results provide relatively reliable chronologic constraints on the origin and evolutionary history of Chenhang Island by using strontium isotope stratigraphy and magnetostratigraphy together. However, further studies are needed to investigate the tectonic, climatic, and sea-level controls on the evolution of the Xisha carbonate platform in the South China Sea.

Geologic Controls on the Development of Coral Reefs

Reef growth is influenced by a variety of biologic (e.g., recruitment, species saturation, competition, predation, symbiosis, and disease) and geologic (substrate availability, antecedent topography, paleoceanographic condition, tectonics, dust input, and changes in atmospheric CO_2 and sea level) factors that act at varying temporal and spatial scales (Daly, 1915; Veron, 1995; Buddemeier, 1997; Buddemeier et al., 1998, 2004; Benzie, 1999; Wood, 1999; Grigg et al., 2002; Vecsei, 2004; Montaggioni, 2005; Hopley et al., 2007; Bar-Or et al., 2008). Unfortunately, there are insufficient data to reconstruct the biologic influences and paleoceanography in the study area. Therefore, we focus on the tectonic subsidence, antecedent topography, dust and terrigenous input, and changes in atmospheric CO_2 and sea level.

The regional unconformity T60 marks the beginning of the postrift stage at ca. 23.8 Ma (Clift and Lin, 2001; Pang et al., 2009). Seismic data suggest that the total subsidence of the Xisha uplift since then is ~2.5 km, and the sedimentation rates in the main depressions of the Xisha uplift generally decreased during the postrift stage (Wu et al., 2014). In our study, the periods of high sedimentation rate were recorded at: 0.21–0.42 Ma, 1.32–1.42 Ma, 1.76–2.73 Ma, 8.74–8.83 Ma, 9.67–10.19 Ma, 15.64–17.12 Ma, 17.44–17.51 Ma, 18.24–18.29, and 18.83–18.88 Ma, respectively (Fig. 9). In particular, the highest sedimentation rate, up to ~740 m/m.y., occurred during 1.39–1.42 Ma (101–121 m), and the second highest value (~428 m/m.y.) occurred during 17.44–17.51 Ma (731–761 m), respectively. The latter is recognized as the warmest episode of the past 25 m.y. Ji et al. (2018) proposed that both the mean value and the variation in CO_2 concentration during the Miocene climatic optimum were elevated compared to the immediately preceding (20.4–17.4 Ma) and following (14–11 Ma) time periods. Furthermore, Nie et al. (2018) demonstrated that increased erosion during a period of high monsoon precipita-tion could have produced rapid incision of the Tibetan Plateau. However, during the Miocene climatic optimum, the eustatic sea level was only 1.6–1.9 m higher than present, and eolian dust accumulation rates also show no large fluctuations (Miller et al., 2005; Guo et al., 2002). In addition, the environment during the Miocene climatic optimum was lagoonal, indicating that the atoll was catching up with the rising sea level. Furthermore, the contribution of input of terrigenous clastics can be neglected because most of the reef sediments are composed of reef-forming organisms and reef-inserted organism either in CK2 or in other wells in the Xisha uplift. Geographically, the Xisha uplift was far away from the siliciclastic sources and has been separated from them by deep-water troughs since the early Miocene. Additionally, siliciclastic input from the Indo-China Peninsula decreased in the middle Miocene, further improving conditions for reef and carbonate platform development in the Xisha region (Wu et al., 2014, and references therein). Hence, we propose that the tectonic subsidence controlled the drowning of coral reefs during this stage. For the interglacial period of 1.39–1.42 Ma, the global sea level was 19.7 m lower than the current sea level (Miller et al., 2005), whereas no important global climate changes were record at this stage. Therefore, rapid subsidence was likely responsible for the highest sedimentation rate during this period. This is a new finding that has not been reported in previous research. In brief, the abnormally high sedimentation rate during these two stages is attributed to the rapid subsidence of basement. Nevertheless, further study is needed for other stages of relatively high sedimentation rates, especially when significant changes in global climate and/or ocean chemistry occurred.

CONCLUSIONS

Based on the comprehensive results of the lithostratigraphic, strontium isotope stratigraphic, magnetostratigraphic, and geochemical analyses, we draw the following conclusions concerning the chronologic constraints on the initiation and evolutionary history of coral reefs in Xisha Island, northern South China Sea:

(1) The petrologic, XRD, and geochemical data show that the reef sequence of CK2 underwent various degrees of diagenetic alteration. However, the diagenetic processes—the conversion from aragonite to calcite, or high-magnesium calcite to low-magnesium calcite, or dolomitization—did not significantly alter the depositional Sr isotope ratios for most of our samples, suggesting that our bulk carbonate samples likely retained primary seawater Sr isotope ratios, or at least near-primary $^{87}Sr/^{86}Sr$ ratios. Careful inspection and pretreatment, integrated utilization of Mn/Sr ratios, Mn concentration, Sr concentration, and $^{18}O/^{16}O$ ratios, and correlations between these proxies further verify the reliability of bulk carbonate to preserve seawater $^{87}Sr/^{86}Sr$. The present $^{87}Sr/^{86}Sr$ results from bulk carbonate suggest that strontium isotope stratigraphy is a powerful tool for dating ancient biotic carbonate.

(2) The Sr data show that the $^{87}Sr/^{86}Sr$ ratio ranges from 0.708506 to 0.709164, corresponding to a numerical age range from 19.20 Ma to 0.35 Ma, suggesting that the reefs started to form at ca. 19.60 Ma at the bottom of the reef sequence. The magnetostratigraphy indicates that the polarity chronozones extend from chron C6 at 866.60 m to present at the top. The impact of diagenetic alteration on the paleomagnetic results appears to have been negligible; however, the influence of low-resolution sampling, changes in SAR, and sedimentary hiatuses complicated detailed correlation between the observed polarity and the GPTS. Our age results clearly point out the initiation time and provide a reliable chronologic framework for the evolutionary process of the Xisha Islands.

(3) We reconstructed the evolutionary history of the reefs since initiation: (a) The reefs initiated in the early Miocene (19.6 Ma) and were drowned until the early middle Miocene (16.26 Ma); (b) during the first development stage (16.26–10.66 Ma), lagoon to lagoon slope environments prevailed; (c) two drowned to development events (10.66–4.36 Ma and 4.36–1.59 Ma, respectively) occurred during 16.26–1.59 Ma. At the end of this stage, the lagoon environment progressively transformed into a reef crest environment. (d) The reef started to be drowned again from the early Pliocene to present (1.59–0 Ma), and the change in environment from lagoon to reef crest or reef flat is attributed to regional structural highs and a moderate rise in relative sea level. Our new chronologic framework for reef evolution in the Xisha Islands can be used as a reliable chronostratigraphy reference for other wells.

REFERENCES CITED

Aïssaoui, D.M., and Kirschvink, J.L., 1991, Atoll magnetostratigraphy: Calibration of their eustatic records: Terra Nova, v. 3, p. 35–40, https://doi.org/10.1111/j.1365-3121.1991.tb00841.x.

Aïssaoui, D.M., McNeil, D.F., and Kirschvink, J.L., 1990, Magnetostratigraphic dating of shallow-water carbonates from Mururoa Atoll, French Polynesia: Implications for global eustasy: Earth and Planetary Science Letters, v. 97, p. 102–112, https://doi.org/10.1016/0012-821X(90)90102-4.

Alexander, I., Andres, M.S., Braithwaite, C.J.R., Braga, J.C., Cooper, M.J., Davies, P.J., Elderfield, P.J., Gilmour, H., Kay, M.A., Kroon, R.L.F., McKenzie, D., Montaggioni, J.A., Skinner, L.F., Thompson, A., Vasconcelos, R., Webster, C.J., Wilson, P.A., and Reef, I.C.G.B., 2001, New constraints on the origin of the Australian Great Barrier Reef: Results from an international project of deep coring: Geology, v. 29, p. 483–486, https://doi.org/10.1130/0091-7613(2001)029<0483:NCOTOO>2.0.CO;2.

Azmy, K., Poty, E., and Brand, U., 2009, High-resolution isotope stratigraphy of the Devonian-Carboniferous boundary in the Namur-Dinant Basin, Belgium: Sedimentary Geology, v. 216, p. 117–124, https://doi.org/10.1016/j.sedgeo.2009.03.002.

Bachan, A., van de Schootbrugge, B., Fiebig, J., McRoberts, C.A., Ciarapica, G., and Payne, J.L., 2012, Carbon cycle dynamics following the end-Triassic mass extinction: Constraints from paired δ13C(carb) and δ13C(org) records: Geochemistry Geophysics Geosystems, v. 13, Q09008, https://doi.org/10.1029/2012GC004150.

Bar-Or, R., Erlick, C., and Gildor, H., 2008, The role of dust in glacial-interglacial cycles: Quaternary Science Reviews, v. 27, p. 201–208, https://doi.org/10.1016/j.quascirev.2007.10.015.

Benzie, J.A.H., 1999, Genetic structure of coral reef organisms: Ghosts of dispersal past: American Zoologist, v. 39, p. 131–145, https://doi.org/10.1093/icb/39.1.131.

Braithwaite, C.J., Dalmasso, H., Gilmour, M.A., Harkness, D.D., Henderson, G.M., Kay, R.L.F., Kroon, D., Montaggioni, L.F., and Wilson, P.A., 2004, The Great Barrier Reef: The chronological record from a new borehole: Journal of Sedimentary Research, v. 74, p. 298–310, https://doi.org/10.1306/091603740298.

Buddemeier, R.W., 1997, Making light work of adaptation: Nature, v. 388, p. 229–230, https://doi.org/10.1038/40755.

Buddemeier, R.W., Gattuso, J.P., and Kleypas, J., 1998, Rising CO$_2$ and marine calcification: Land-Ocean Interactions in the Coastal Zone Project Newsletter, v. 8, p. 1–3.

Buddemeier, R.W., Kleypas, J.A., and Aronson, R.B., 2004, Coral Reefs and Global Climate Change: Potential Contributions of Climate Change to Stresses on Coral Reef Ecosystems: Arlington, Pew Center on Global Climate Change, Report, February, 42 p.

Burke, W.H., Denison, R.E., Hetherington, E.A., Koepnick, R.B., Nelson, H.F., and Otto, J.B., 1982, Variation of seawater ⁸⁷Sr/⁸⁶Sr throughout Phanerozoic time: Geology, v. 10, p. 516–519, https://doi.org/10.1130/0091-7613(1982)10<516:VOSSTP>2.0.CO;2.

Cabioch, G., Montaggioni, L., Thouveny, N., Frank, N., Sato, T., Chazottes, V., Dalamasso, H., Payri, C., Pichon, M., and Semah, A.M., 2008, The chronology and structure of the western New Caledonian barrier reef tracts: Palaeogeography, Palaeoclimatology, Palaeoecology, v. 268, p. 91–105, https://doi.org/10.1016/j.palaeo.2008.07.014.

Clift, P.D., and Lin, J., 2001, Preferential mantle lithospheric extension under the South China margin: Marine and Petroleum Geology, v. 18, p. 929–945, https://doi.org/10.1016/S0264-8172(01)00037-X.

Clift, P.D., and Sun, Z., 2006, The sedimentary and tectonic evolution of the Yinggehai-Song Hong basin and the southern Hainan margin, South China Sea: Implications for Tibetan uplift and monsoon intensification: Journal of Geophysical Research–Solid Earth, v. 111, no. B6, B06405, https://doi.org/10.1029/2005JB004048.

Daly, R.A., 1915, The glacial control theory of coral reefs: Proceedings of the American Academy of Arts and Sciences, v. 51, p. 155–251, https://doi.org/10.2307/20025572.

DePaolo, D.J., 1986, Detailed record of the Neogene Sr isotopic evolution of seawater from DSDP Site 590B: Geology, v. 14, p. 103–106, https://doi.org/10.1130/0091-7613(1986)14<103:DROTNS>2.0.CO;2.

DePaolo, D.J., and Ingram, B.L., 1985, High-resolution stratigraphy with strontium isotopes: Science, v. 227, p. 938–941, https://doi.org/10.1126/science.227.4689.938.

Derry, L.A., Keto, L.S., Jacobsen, S.B., Knoll, A.H., and Swett, K., 1989, Sr isotopic variations in Upper Proterozoic carbonates from Svalbard and East Greenland: Geochimica et Cosmochimica Acta, v. 53, p. 2331–2339, https://doi.org/10.1016/0016-7037(89)90355-4.

Derry, L.A., Kaufman, A.J., and Jacobsen, S.B., 1992, Sedimentary cycling and environmental change in the late Proterozoic: Evidence from stable and radiogenic isotopes: Geochimica et Cosmochimica Acta, v. 56, p. 1317–1329, https://doi.org/10.1016/0016-7037(92)90064-P.

Edwards, C.T., Saltzman, M.R., Leslie, S.A., Bergstrom, S.M., Sedlacek, A.R.C., Howard, A., Bauer, J.A., Sweet, W.C., and Young, S.A., 2015, Strontium isotope (Sr-87/Sr-86) stratigraphy of Ordovician bulk carbonate: Implications for preservation of primary seawater values: Geological Society of America Bulletin, v. 127, p. 1275–1289, https://doi.org/10.1130/B31149.1.

Elderfield, H., 1986, Strontium isotope stratigraphy: Palaeogeography, Palaeoclimatology, Palaeoecology, v. 57, p. 71–90, https://doi.org/10.1016/0031-0182(86)90007-6.

Faichney, I.D.E., Webster, J.M., Clague, D.A., Paduan, J.B., and Fullager, P.D., 2013, Unraveling the tilting history of the submerged reefs surrounding Oahu and the Maui-Nui Complex, Hawaii: Geochemistry Geophysics Geosystems, v. 11, Q07002, https://doi.org/10.1029/2010gc003044.

Fyhn, M.B.W., Boldreel, L.O., Nielsen, L.H., Giang, T.C., Le, H.N., Hong, N.T.M., Nguyen, N.D., and Abatzis, I., 2013, Carbonate platform growth and demise offshore Central Vietnam: Effects of Early Miocene transgression and subsequent onshore uplift: Journal of Asian Earth Sciences, v. 76, p. 152–168, doi:j.jseaes.2013.02.023.

Gieskes, J.M., Elderfield, H., Palmer, M.R., 1986, Strontium and its isotopic composition in interstitial waters of marine carbonate sediments: Earth and Planetary Science Letters, v. 77, p. 229–235, https://doi.org/10.1016/0012-821X(86)90163-9.

Grigg, R.W., Grossman, E.E., Earle, S.A., Gittings, S.R., Lotts, D., and McDonough, J., 2002, Drowned reefs and antecedent karst topography, Au'au Channel, S.E. Hawaiian Islands: Coral Reefs, v. 21, p. 73–82, https://doi.org/10.1007/s00338-001-0203-8.

Guo, Z.T., Ruddiman, W.F., Hao, Q.Z., Wu, H.B., Qiao, Y.S., Zhu, R.X., Peng, S.Z., Wei, J.J., Yuan, B.J., and Liu, T.S., 2002, Onset of Asian desertification by 22 Myr ago inferred from loess deposits in China: Nature, v. 416, p. 159–163, https://doi.org/10.1038/416159a.

Halverson, G.P., Dudás, F.O., Maloof, A.C., and Bowring, S.A., 2007, Evolution of the ⁸⁷Sr/⁸⁶Sr composition of Neoproterozoic seawater: Palaeogeography, Palaeoclimatology, Palaeoecology, v. 256, p. 103–129, https://doi.org/10.1016/j.palaeo.2007.02.028.

Hayes, J.M., Strauss, H., and Kaufman, A.J., 1999, The abundance of C-13 in marine organic matter and isotopic fractionation in the global biogeochemical cycle of carbon during the past 800 Ma: Chemical Geology, v. 161, p. 103–125, https://doi.org/10.1016/S0009-2541(99)00083-2.

He, Q.X., Zhang, M.S., Ye, Z.J., Han, C.D., Wu, J.Z., Li, H.J., and Lian, J., 1986, Oxygen isotope stratigraphy of late Pleistocene carbonate deposits at Shidao, Xisha Islands, China: Marine Geology & Quaternary Geology [Haiyang Dizhi Yu Disiji Dizhi], v. 6, p. 1–8 [in Chinese with English abstract].

Hess, J., Bender, M.L., and Schilling, J.G., 1986, Evolution of the ratio of strontium-87 to strontium-86 in seawater from Cretaceous to present: Science, v. 231, p. 979–984, https://doi.org/10.1126/science.231.4741.979.

Hopley, D., Smithers, S.G., and Parnell, K.E., 2007, The Geomorphology of the Great Barrier Reef: Development, Diversity, and Change: Cambridge, UK, Cambridge University Press, 532 p., https://doi.org/10.1017/CBO9780511535543.

Hua, Q., 2009, Radiocarbon: A chronological tool for the recent past: Quaternary Geochronology, v. 4, p. 378–390, https://doi.org/10.1016/j.quageo.2009.03.006.

Huang, D.W., Licuanan, W.Y., Hoeksema, B.W., Chen, C.L.A., Ang, P.O., Huang, H., Lane, D.J.W., Vo, S.T., Waheed, Z., Affendi, Y.A., Yeemin, T., and Chou, L.M., 2015, Extraordinary diversity of reef corals in the South China Sea: Marine Biodiversity, v. 45, p. 157–168, https://doi.org/10.1007/s12526-014-0236-1.

Ji, S.C., Nie, J.S., Lechler, A., Huntiington, K.W., Heitmann, E.O., and Breecker, D.O., 2018, A symmetrical CO$_2$ peak and asymmetrical climate change during the middle Miocene: Earth and Planetary Science Letters, v. 499, p. 134–144, https://doi.org/10.1016/j.epsl.2018.07.011.

Kaufman, A.J., Knoll, A.H., and Awramik, S.M., 1992, Biostratigraphic and chemostratigraphic correlation of Neoproterozoic sedimentary successions: Upper Tindir Group, northwestern Canada, as a test case: Geology, v. 20, p. 181–185, https://doi.org/10.1130/0091-7613(1992)020<0181:BACCON>2.3.CO;2.

Kaufman, A.J., Jacobsen, S.B., and Knoll, A.H., 1993, The Vendian record of Sr and C isotopic variations in seawater: Implications for tectonics and paleoclimate: Earth and Planetary Science Letters, v. 120, p. 409–430, https://doi.org/10.1016/0012-821X(93)90254-7.

Kiessling, W., 2009, Geologic and biologic controls on the evolution of reefs: Annual Review of Ecology Evolution and Systematics, v. 40, p. 173–192, https://doi.org/10.1146/annurev.ecolsys.110308.120251.

Kirschvink, J.L., 1980, The least-squares line and plane and the analysis of palaeomagnetic data: Geophysical Journal of the Royal Astronomical Society, v. 62, p. 699–718, https://doi.org/10.1111/j.1365-246X.1980.tb02601.x.

Korte, C., Kozur, H.W., Bruckschen, P., and Veizer, J., 2003, Strontium isotope evolution of Late Permian and Triassic seawater: Geochimica et Cosmochimica Acta, v. 67, p. 47–62, https://doi.org/10.1016/S0016-7037(02)01035-9.

Li, D., Shields-Zhou, G.A., Ling, H.F., and Thirlwall, M., 2011, Dissolution methods for strontium isotope stratigraphy: Guidelines for the use of bulk carbonate and phosphorite rocks: Chemical Geology, v. 290, p. 133–144, https://doi.org/10.1016/j.chemgeo.2011.09.004.

Lincoln, J.M., and Schlanger, S.O., 1991, Atoll stratigraphy as a record of sea level change: Problems and prospects: Journal of Geophysical Research–Solid Earth, v. 96, p. 6727–6752, https://doi.org/10.1029/90JB00601.

Liu, C., Wang, Z.R., and Raub, T.D., 2013, Geochemical constraints on the origin of Marinoan cap dolostones from Nuccaleena Formation, South Australia: Chemical Geology, v. 351, p. 95–104, https://doi.org/10.1016/j.chemgeo.2013.05.012.

Lu, G., Aharon, P., Wheeler, C.W., and McCabe, C., 1996, Magnetostratigraphy of the uplifted former atoll of Niue, South Pacific: Implications for accretion history and carbonate diagenesis: Sedimentary Geology, v. 105, p. 259–274, https://doi.org/10.1016/0037-0738(96)00014-0.

Ludwig, K.R., Halley, R.B., Simmons, K.R., and Peterman, Z.E., 1988, Strontium-isotope stratigraphy of Enewetak Atoll: Geology, v. 16, p. 173–177, https://doi.org/10.1130/0091-7613(1988)016<0173:SISOEA>2.3.CO;2.

Lund, S., Platzman, E., Thouveny, N., Camoin, G., Corsetti, F., and Berelson, W., 2010, Biological control of paleomagnetic remanence acquisition in carbonate framework rocks of the Tahiti coral reef: Earth and Planetary Science Letters, v. 298, p. 14–22, https://doi.org/10.1016/j.epsl.2010.07.010.

Ma, Y.B., Wu, S.G., Lv, F.L., Dong, D.D., Sun, Q.L., Lu, Y.T., and Gu, M.F., 2011, Seismic characteristics

and development of the Xisha carbonate platforms, northern margin of the South China Sea: Journal of Asian Earth Sciences, v. 40, p. 770–783, https://doi.org/10.1016/j.jseaes.2010.11.003.

McArthur, J.M., Howarth, R.J., and Bailey, T.R., 2001, Strontium isotope stratigraphy: LOWESS version 3: Best fit to the marine Sr-isotope curve for 0–509 Ma and accompanying look-up table for deriving numerical age: The Journal of Geology, v. 109, p. 155–170, https://doi.org/10.1086/319243.

McNeill, D.F., Ginsburg, R.N., Chang, S.B.R., and Kirschvink, J.L., 1988, Magnetostratigraphic dating of shallow-water carbonates from San Salvador, Bahamas: Geology, v. 16, p. 8–12, https://doi.org/10.1130/0091-7613(1988)016<0008:MDOSWC>2.3.CO;2.

Ménabréaz, L., Thouveny, N., Camoin, G., and Lund, S.P., 2010, Paleomagnetic record of the late Pleistocene reef sequence of Tahiti (French Polynesia): A contribution to the chronology of the deposits: Earth and Planetary Science Letters, v. 294, p. 58–68, https://doi.org/10.1016/j.epsl.2010.03.002.

Miller, K.G., Kominz, M.A., Browning, J.V., Wright, J.D., Mountain, G.S., Katz, M.E., Sugarman, P.J., Cramer, B.S., Christie-Blick, N., and Pekar, S.F., 2005, The Phanerozoic record of global sea-level change: Science, v. 310, p. 1293–1298, https://doi.org/10.1126/science.1116412.

Montaggioni, L.F., 2005, History of Indo-Pacific coral reef systems since the last glaciation: Development patterns and controlling factors: Earth-Science Reviews, v. 71, p. 1–75, https://doi.org/10.1016/j.earscirev.2005.01.002.

Montañez, I.P., Banner, J.L., Osleger, D.A., Borg, L.E., and Bosserman, P.J., 1996, Integrated Sr isotope variations and sea-level history of Middle to Upper Cambrian platform carbonates: Implications for the evolution of Cambrian seawater $^{87}Sr/^{86}Sr$: Geology, v. 24, p. 917–920, https://doi.org/10.1130/0091-7613(1996)024<0917:ISIVAS>2.3.CO;2.

Nie, J.S., Ruetenik, G., Gallagher, K., Hoke, G., Garzione, C., Wang, W.T., Stockli, D., Hu, X.F., Wang, Z., Wang, Y., Stevens, T., Danišík, M., and Liu, S.P., 2018, Rapid incision of the Mekong River in the middle Miocene linked to monsoonal precipitation: Nature Geoscience, v. 11, p. 944–948, https://doi.org/10.1038/s41561-018-0244-z.

Ogg, J.G., 2012, Geomagnetic polarity time scale, *in* Gradstein, F.M., Ogg, J.G., Schmitz, M.D., and Ogg, G.M., eds., The Geologic Time Scale: Boston, Massachusetts, Elsevier, p. 85–113, https://doi.org/10.1016/B978-0-444-59425-9.00005-6.

Ohde, S., and Elderfield, H., 1992, Strontium isotope stratigraphy of Kita-daito-jima Atoll, North Philippine Sea: Implications for Neogene sea-level change and tectonic history: Earth and Planetary Science Letters, v. 113, p. 473–486, https://doi.org/10.1016/0012-821X(92)90125-F.

Ohde, S., Greaves, M., Masuzawa, T., Buckley, H.A., Van Woesik, R., Wilson, P.A., Pirazzoli, P.A., and Elderfield, H., 2002, The chronology of Funafuti Atoll: Revisiting an old friend: Proceedings of the Royal Society, Mathematical, Physical and Engineering Sciences, v. 458, p. 2289–2306, https://doi.org/10.1098/rspa.2002.0978.

Palmer, M.R., and Elderfield, H., 1985, Sr isotope composition of sea water over the past 75 Myr: Nature, v. 314, p. 526–528, https://doi.org/10.1038/314526a0.

Pandolfi, J.M., 2015, Incorporating uncertainty in predicting the future response of coral reefs to climate change: Annual Review of Ecology Evolution and Systematics, v. 46, p. 281–303, https://doi.org/10.1146/annurev-ecolsys-120213-091811.

Pang, X., Chen, C., Zhu, M., He, M., Shen, J., Lian, S., and Wu, X., 2009, Baiyun movement: A significant tectonic event on the Oligocene/Miocene boundary in the northern South China Sea and its regional implications: Journal of Earth Science, v. 20, p. 49–56, https://doi.org/10.1007/s12583-009-0005-4.

Qin, G.Q., 1987, A preliminary study on foraminiferal assemblages of well 1 Xiyong, Xisha Islands and their coral reef formation: Tropic Oceanology [Redai Haiyang], v. 6, p. 10–20 [in Chinese with English abstract].

Qiu, Y., and Wang, Y.M., 2001, Reefs and paleostructure and paleoenvironment in the South China Sea: Marine Geology & Quaternary Geology [Haiyang Dizhi Yu Disiji Dizhi], v. 21, p. 65–73 [in Chinese with English abstract].

Quinn, T.M., Lohmann, K.C., and Halliday, A.N., 1991, Sr isotope variation in shallow water carbonate sequence: Stratigraphic, chronostratigraphic, and eustatic implications of the record at Enewetak Atoll: Paleoceanography, v. 6, p. 371–385, https://doi.org/10.1029/91PA00384.

Saller, A.H., and Koepnick, R.B., 1990, Eocene to early Miocene growth of Enewetak Atoll: Insight from strontium-isotope data: Geological Society of America Bulletin, v. 102, p. 381–390, https://doi.org/10.1130/0016-7606(1990)102<0381:ETEMGO>2.3.CO;2.

Sasaki, K., Omura, A., Miwa, T., Tsuji, Y., Matsuda, H., Nakamori, T., Iryu, Y., Yamada, T., Sato, Y., and Nakagawa, H., 2006, Th-230/U-234 and C-14 dating of a lowstand coral reef beneath the insular shelf off Irabu Island, Ryukyus, southwestern Japan: The Island Arc, v. 15, p. 455–467, https://doi.org/10.1111/j.1440-1738.2006.00541.x.

Scasso, R.A., and Kiessling, W., 2001, Diagenesis of Upper Jurassic concretions from the Antarctic Peninsula: Journal of Sedimentary Research, v. 71, p. 88–100, https://doi.org/10.1306/032800710088.

Shao, L., Li, Q.Y., Zhu, W.L., Zhang, D.J., Qiao, P.J., Liu, X.Y., You, L., Cui, Y.C., and Dong, X.X., 2017, Neogene carbonate platform development in the NW South China Sea: Litho-, bio- and chemo-stratigraphic evidence: Marine Geology, v. 385, p. 233–243, https://doi.org/10.1016/j.margeo.2017.01.009.

Sun, Z.G., Liu, B.Z., Liu, J., Lan, X.H., Wu, J.Z., Zhou, M.Q., Han, C.R., and Ye, Y.G., 1996, The characteristics of Sr isotope ratios and its paleoenvironmental significance: Chinese Science Bulletin, v. 41, p. 434–437 [in Chinese with English abstract].

Vahrenkamp, V.C., Swart, P.K., and Ruiz, J., 1988, Constraints and interpretation of $^{87}Sr/^{86}Sr$ ratios in Cenozoic dolomites: Geophysical Research Letters, v. 15, p. 385–388, https://doi.org/10.1029/GL015i004p00385.

Vecsei, A., 2004, A new estimate of global reefal carbonate production including the fore-reefs: Global and Planetary Change, v. 43, p. 1–18, https://doi.org/10.1016/j.gloplacha.2003.12.002.

Veizer, J., 1989, Strontium isotopes in seawater through time: Annual Review of Earth and Planetary Sciences, v. 17, p. 141–167, https://doi.org/10.1146/annurev.ea.17.050189.001041.

Veron, J.E.N., 1995, Corals in Space and Time: The Biogeography and Evolution of the Scleractinia: Sydney, Australia, University of South Wales Press, 321 p., https://doi.org/10.1086/419409.

Wang, P.X., and Li, Q.Y., eds., 2009, The South China Sea: Paleoceanography and Sedimentology: Dordrecht, Netherlands, Springer, Developments in Paleoenvironmental Research 13, 506 p., https://doi.org/10.1007/978-1-4020-9745-4.

Wang, R., Yu, K.F., Jones, B., Wang, Y.H., Zhao, J.X., Feng, Y.X., Bian, L.Z., Xu, S.D., Fan, T.L., Jiang, W., and Zhang, Y., 2018, Evolution and development of Miocene "island dolostones" on Xisha Islands, South China Sea: Marine Geology, v. 406, p. 142–158, https://doi.org/10.1016/j.margeo.2018.09.006.

Webster, J.M., Clague, D.A., Faichney, I.D.E., Fullagar, P.D., Hein, J.R., Moore, J.G., and Paull, C.K., 2010, Early Pleistocene origin of reefs around Lanai, Hawaii: Earth and Planetary Science Letters, v. 290, p. 331–339, https://doi.org/10.1016/j.epsl.2009.12.029.

Wei, X., Xu, Y.G., Feng, Y.X., and Zhao, J.X., 2014, Plume-lithosphere interaction in the generation of the Tarim large igneous province, NW China: Geochronological and geochemical constraints: American Journal of Science, v. 314, p. 314–356, https://doi.org/10.2475/01.2014.09.

Wilson, P.A., Jenkyns, H.C., Elderfield, H., and Larson, R.L., 1998, The paradox of drowned carbonate platforms and the origin of Cretaceous Pacific guyots: Nature, v. 392, p. 889–894, https://doi.org/10.1038/31865.

Wood, R., 1999, Reef Evolution: New York, Oxford University Press, 414 p.

Wu, S.G., Yang, Z., Wang, D.W., Lu, F.L., Ludmann, T., Fulthorpe, C., and Wang, B., 2014, Architecture, development and geological control of the Xisha carbonate platforms, northwestern South China Sea: Marine Geology, v. 350, p. 71–83, https://doi.org/10.1016/j.margeo.2013.12.016.

Wu, S.Q., Zhang, X.Y., Yang, Z., Wu, T.Y., Gao, J.W., and Wang, D.W., 2016, Spatial and temporal evolution of Cenozoic carbonate platforms on the continental margins of the South China Sea: Response to opening of the ocean basin: Interpretation—A Journal of Subsurface Characterization, v. 4, p. SP1–SP19, https://doi.org/10.1190/INT-2015-0162.1.

Xu, G.Q., Lü, B.Q., and Wang, H.G., 2002, Drowning events research: Insight from Cenozoic carbonate platform in northern South China Sea: Journal of Tongji University, v. 30, p. 35–40 [in Chinese with English abstract].

Yi, L., Wang, Z.F., Zhang, D.J., Liu, X.Y., You, L., Luo, W., Zhu, Y.H., Qin, H.F., and Deng, C.L., 2016, Magnetostratigraphy of biogenic reef in the Sanya Formation of borehole XK-1 from Xisha Islands and its environmental significance: Coastal Engineering, v. 35, p. 1–11 [in Chinese with English abstract].

Yi, L., Jian, Z., Liu, X., Zhu, Y., Zhang, D., Wang, Z., and Deng, C., 2018, Astronomical tuning and magnetostratigraphy of Neogene biogenic reefs in Xisha Islands: South China Sea: Science Bulletin, v. 63, p. 564–573, https://doi.org/10.1016/j.scib.2018.04.001.

Young, S.A., Saltzman, M.R., Foland, K.A., Linder, J.S., and Kump, L.R., 2009, A major drop in seawater $^{87}Sr/^{86}Sr$ during the Middle Ordovician (Darriwilian): Links to volcanism and climate?: Geology, v. 37, p. 951–954, https://doi.org/10.1130/G30152A.1.

Zhang, M.S., 1990, Discovery of Xisha event cycle and significance: Marine Geology & Quaternary Geology [Haiyang Dizhi Yu Disiji Dizhi], v. 10, p. 83–90 [in Chinese with English abstract].

Zhang, M.S., He, Q.X., Zheng, Y.Z., Han, C.R., Li, H., Wu, J.Z., and Ju, L.J., 1989, The Research of Sediment Geology of Carbonate Platform in Xisha: Beijing, Science Press, 117 p.

Zhang, M.S., Liu, J., and Zhou, M.Q., 1996, The magnetostratigraphy of Xisha well: Marine Geology & Quaternary Geology [Haiyang Dizhi Yu Disiji Dizhi], v. 16, p. 61–65 [in Chinese with English abstract].

Zhang, Y., Yu, K.F., and Qian, H.D., 2018, LA-ICP-MS analysis of clinopyroxenes in basaltic pyroclastic rocks from the Xisha Islands, northwestern South China Sea: Minerals (Basel), v. 8, p. 575, https://doi.org/10.3390/min8120575.

Zhang, Y., Yu, K.F., Qian, H.D., Fan, T.L., Yue, Y.F., Wang, R., Jiang, W., Xu, S.D., and Wang, Y.H., 2019, The basement and volcanic activities of the Xisha Islands: Evidence from the kilometre-scale drilling in the northwestern South China Sea: Geological Journal (in press), https://doi.org/10.1002/gj.3416.

Zijderveld, J.D.A., 1967, AC demagnetization of rocks: Analysis of results, *in* Runcorn, S.K., Creer, K.M., and Collinson, D.W., eds., Methods in Palaeomagnetism: Amsterdam, Netherlands, Elsevier, p. 254–286.